Study of Soft X-Ray Yield from NX2 Plasma Focus Using Lee Model Code

A Dissertation

Submitted to the Department of Physics
Birendra Multiple Campus, Tribhuvan University
Bharatpur, Chitwan, Nepal
in the Partial Fulfillment for the Requirement of
Master's Degree of Science in Physics

By

Prakash Gautam

May, 2014

Contents

Recommendation **i**

Evaluation **ii**

Abstract **iii**

Acknowledgements **iv**

List of Tables **vi**

List of Figures **vii**

1 Introduction **1**

1.1 Introduction to Plasma 2

1.1.1 Debye shielding 3

1.1.2 Plasma frequency 4

1.1.3 Criteria for plasma 6

1.2 Thermonuclear Fusion 6

1.3 Dawning Towards Plasma Focus 9

1.4 Plasma Focus as X-rays Emitter 15

1.5 Merits of Plasma X-ray 16

1.6 Scope and Layout 16

2 Review of Plasma Focus Studies **18**

3 Plasma Focus and Lee Model Code **25**

3.1 Dense Plasma Focus and Lee Model Code 26

3.1.1 Axial phase 30

3.1.2 Radial inward shock phase 30

3.1.3 Radial reflected shock phase 31

3.1.4 Slow compression (Quiescent) or pinch phase 31

3.1.5 Expanded column phase 32

4 Theoretical Model of Plasma Focus **33**

4.1 Description of Model 34

4.2 Axial Phase 35

4.2.1 Equation of motion(Snow-Plow model) 35

4.2.2 Circuit (Current) equation: 36

4.3 Radial Phase 39

4.3.1 Radial inward shock phase 41

4.3.2 Radial reflected shock phase 46

4.3.3 Slow compression phase 47

4.3.4 Expanded column axial phase 48

4.4 NX2 Plasma Focus Device 49

5 Results and Discussion **52**

6 Conclusion and Future Works **65**

6.1 Conclusion 66

6.2 Future Works 67

Bibliography **69**

RECOMMENDATION

It is certified that **Mr. Prakash Gautam** has carried out the dissertation work entitled **Study of Soft X-ray Yield from NX2 Plasma Focus Using Lee Model Code** under our supervision.

We recommend the dissertation in the partial fulfillment for the requirement of Master's Degree of Science in Physics at Tribhuvan University.

(Dr. Raju Khanal)
Supervisor
Central Department of Physics
Tribhuvan University, Kirtipur
Kathmandu, Nepal

(Mr. Ram Krishna Tiwari)
Supervisor
Department of Physics
Birendra Multiple Campus
Bharatpur, Chitwan

Date : ——————

EVALUATION

We certify that we have evaluated this dissertation entitled **Study of Soft X-ray Yield from NX2 Plasma Focus Using Lee Model Code** submitted by **Mr. Prakash Gautam** and in our opinion, it fulfills all the specified criteria, in the scope and quality, as a dissertation for the partial fulfillment of the requirement for the degree of Master of Science in Physics at Tribhuvan University, Kirtipur, Kathmandu, Nepal.

Evaluation Committee

(Dr. Raju Khanal)
Supervisor
Central Department of Physics
Tribhuvan University, Kirtipur
Kathmandu, Nepal

(Mr. Ram Krishna Tiwari)
Supervisor
Department of Physics
Birendra Multiple Campus
Bharatpur, Chitwan

External Examiner

Internal Examiner

(Mr. Arun Kumar Shrestha)
Head, Department of Physics
Birendra Multiple Campus
Bharatpur, Chitwan

Date:.....

ABSTRACT

A Dense Plasma Focus (DPF) is a table top device producing a short-lived very hot plasma and can cause nuclear fusion. Lee Model Code is a computer simulation package, which has been successfully used in studying various PF devices across the world.

In the present work we have used the Lee Code to study the neon soft x-ray emitted from the NX2 PF device; which is a four-model Singaporean 3kJ neon PF designed for SXR lithography. Numerical experiments are mainly carried out under various operating pressure of gas with other parameter adjusted to the values of lab. Our objective is to correlate the plasma dynamics and the time periods of the plasma device with some other emission parameters. The NX2 device is operated with 11 kV in the computer simulation package and we compare the computed data with the published measured data. In our study computed values agree with the measured value. The result states that the neon soft x-ray yield is maximum at the pressure of 2.9 Torr and is 22.6 Joule/shot, whereas the maximum value was at 3.31 Torr at the laboratory and measured by Zhang. Computed current curves versus pressure are presented and discussed particularly in terms the dynamic resistance and the computed gross properties are presented and the variation of these plasma dynamics are discussed to explain the maximization of the Y_{sxr} at the optimum pressure.

This result obtained is expected to be useful in the area of microlithography, micromachining, materials modification and fabrication, imaging and medical and astrophysical simulation together with modelling and computation. Our result agree with the previous work [22] with slight change in other plasma dynamics.

ACKNOWLEDGEMENTS

I offer my sincerest gratitude to my supervisors, Dr. Raju Khanal and Mr. Ram Krishna Tiwari. I have been amazingly fortunate to have supervisors who gave me the freedom to explore on my own, and at the same time the guidance to recover when my steps faltered, together with teaching me how to question thoughts and express ideas. Their patience and support helped me overcome many difficult situations and finish this dissertation. I could not have imagined having a better supervisors and mentors for my Masters degree study.

I would like to pay my heartfelt thanks to Mr. Arun Kumar Shrestha, Head of the Department of Physics, Birendra Multiple Campus, Bharatpur, Chitwan and Prof. Dr. Binil Aryal, Head of the Central Department of Physics, Tribhuvan University, Kirtipur, for their valuable suggestion and encouragement throughout the work. I am grateful to my faculty teachers at the Central Department of Physics, special thanks Prof. Dr. L. N Jha for his valuable suggestion and teachers at Birendra Multiple Campus: Prof. Dr. S. B Thapa, Prof. Dr. Harihar Poudel, Dr. Keshav Bhakta Sapkota, Mr. Dilli Prasad Sharma, Mr. Arun Kumar Sah, Dr. Sheskanta Adhikari, Mr. Udaya Bahadur Thapa, Mr. Moti Bhusal, Mr. Rabindra Raj Bista, Mr. Pratap Koirala, Mr. Netra Bhurtel, Mr. Rajendra Neupane, Mr. Ishwor Chandra Pokhrel, Mr. Madan Fuyal and Mr. Bijay Pandit for their valuable suggestions and intellectual support throughout the work.

My special appreciation goes to Prof. Dr. Lee Sing and Prof. Dr. Saw Sor Heoh for introducing, teaching and also providing the Model Code. Furrthermore Prof. Lee helped me by replying all my queries and providing reference materials related to my work. I am also thankful to Prof. Dr. Deepak Subedi for fruitful discussions.

My friends who directly or indirectly helped me for my work - lots of thanks.

Last but not least, I owe more than thanks to all to my family members for their support and encouragement throughout my life.

List of Tables

1.1 - Comparison of PF device with ITER 14

5.1 - Computed plasma dynamics and pinch plasma parameters 59

5.2 - Computed plasma dynamics and pinch plasma parameters 60

5.3 - Real experimental data of Y_{sxr} 61

List of Figures

1.1 - Examples of plasmas 3

1.2 - Debye shielding 5

1.3 - Deuterium-Tritium fusion reaction 7

1.4 - Energy sources 10

1.5 - Scenario of energy consumption 11

1.6 - Scenario of energy consumption 12

3.1 - Schematic arrangement of PF electrodes system and diagnostics 27

3.2 - Dense plasma focus device 28

3.3 - Shadow-graphic sequences 28

3.4 - Illustration of two phases of a PF 30

4.1 - Simplified process 34

4.2 - Schematic of radius versus time trajectories 40

4.3 - Schematic of the electrical system and focus electrodes with chamber 51

5.1 - Total current waveform versus time 54

5.2 - Effect on key pinch plasma parameters 56

5.3 - Y_{sxr} versus neon pressure 57

5.4 - Radial phases/phenomenon versus time 58

5.5 - Axial trajectories and speed versus time 62

5.6 - The tube voltage versus time 63

5.7 - Plasma temperature versus time 64

Chapter 1

Introduction

1.1 Introduction to Plasma

A key part of the science of fusion is plasma physics. In the mid-19th century Czech physiologist Jan Evangelista Purkinje introduced use of the Greek word plasma (meaning "formed or molded or febricated") to denote the clear fluid which remains after removal of all the corpuscular material in blood [1]. Irving Langmuir and collaborators were the first to study phenomena in plasma in the early 1920's while working on the development of vacuum tubes for large currents and the term plasma was first introduced in physics by Irving Langmuir (1929) to describe the state of matter in the positive column of glow discharge tube [2]. The distinct nature of ionized gases were first observed by Sir William Crooks in 1879 and he named it as the "radiant" or "4^{th} state" of matter [3].

It has often been said that about 99 % of the matter in the Universe is in plasma state. The stellar interiors and atmospheres, gaseous nebula, interstellar hydrogens, solar winds are plasmas. We live in the remaining 1 % of the Universe in which plasmas do not occur naturally. In our own neighborhood, as soon as one leaves the earth's atmosphere, one encounter the plasma comprising the Van Allen radiation belts and the solar wind. In our everyday life encounters with the limited number of the plasmas as examples: flash of the lightening bolt, neon sign, soft glow of the Aurora Borealis, and the slight amount of ionization in a rocket exhaust [4]. Some of the examples of plasma are shown in Figure 1.1.

When a gas is raised to sufficiently high temperature, its constituents (atoms or molecules) become thermally agitated and therefore collide violently. Consequently, the electrons are stripped off and the atoms becomes ionized [5]. Characteristic electrical oscillations of very high frequency can exist in an ionized gas that is neutral or Quasi-neutral particles which exhibits collective behavior [6].

Plasma is the state attained by ionized gases but all ionized gases can't be called plasma.

Plasma is Quasi-neutral gas of charged and neutral particles, which exhibits collective behaviors [4]. Quasi-neutrality of plasma implies that the electron and ion density are nearly equal so that we take $n_i \simeq n_e \simeq n$, where n is the common density called plasma density but not so neutral that all the interesting electromagnetic forces vanish. Collective behavior of plasma implies that the motion of the ion depends not only on the local conditions but also on the state of plasma far away from the point of interest [4, 7]. To further define the plasma

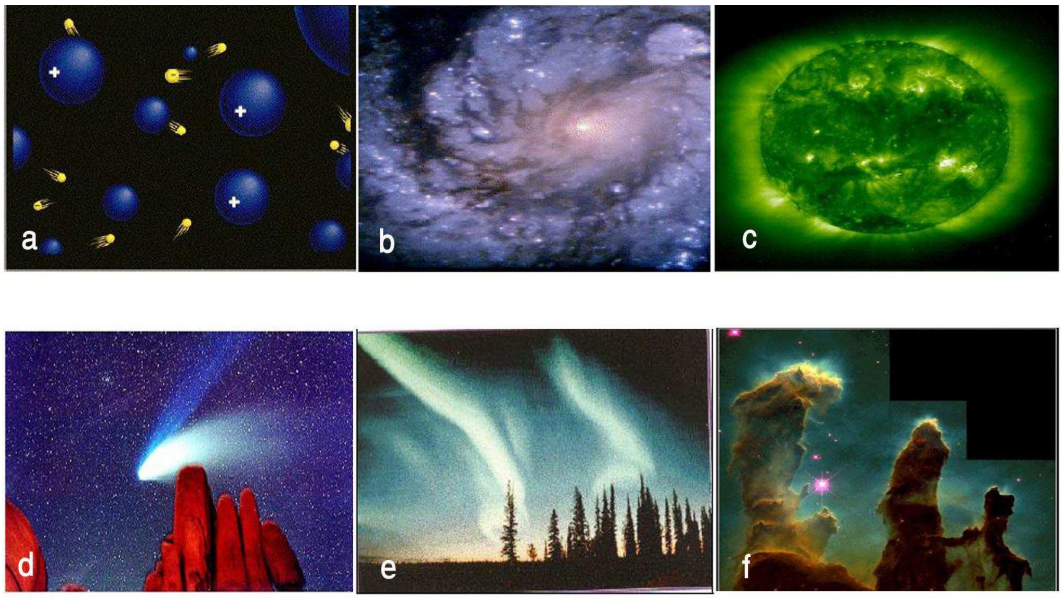

Figure 1.1: *Examples of plasmas a) Plasma formed by ions and electrons, b) Spiral galaxies as plasma, c) Most of the sun is in plasma state, especially the corona, d) Comet tails as the dusty plasmas, e) Aurora Borealis as a cooler plasma, f) Plasmas at the birth of stars in nebula [8].*

state it will useful to discuss some basic related terms.

1.1.1 Debye shielding

Plasma sheaths are the boundary layers formed between a plasma and a boundary surface, where the electron and ion densities are different. The thickness of the plasma sheath is known to be of the order of a quantity called the "Debye length". A fundamental property

of plasma is its ability to shield out electric potential that are applied to it and where the potential is shielded within very small region is shown in Figure 1.2, there by reducing the effectiveness of the test particle's field beyond the Debye length [4]. Typical relations for the electron Debye length (λ_D) is,

$$\lambda_D = \sqrt{\frac{\epsilon_o k_B T_e}{e^2 n_e}}. \tag{1.1}$$

where, n_e is electron density, T_e is electron temperature, e is electronic charge, k_B is the Boltzmann constant and ϵ_o is the permittivity of vacuum. A sphere of radius equal to λ_D inside a plasma is called a Debye sphere. Any electrostatic field originated outside a Debye sphere is effectively screened by the charged particles and does not contribute to electric field existing at its center. Consequently, each charge in the plasma interacts collectively only with the charges those lie inside its Debye sphere, its effect on the other charges being effectively negligible. The number of electrons in a Debye sphere is given by [4].

$$N_D = \frac{4}{3}\pi {\lambda_D}^3 n_e = \frac{4\Pi}{3\sqrt{n}}(\frac{\epsilon_o k_B T_e}{e^2})^{3/2} \tag{1.2}$$

1.1.2 Plasma frequency

If the electrons in a plasma are displaced form a uniform background of ions, electric field will be built in such a direction as to restore the neutrality of the plasma by pulling the electrons back to their original positions. Because of the inertia, the electrons will overshoot and oscillate about their equilibrium positions with a characteristic frequency known as plasma frequency. This oscillation is so fast that the massive ions do not have time to respond to the oscillating electric field and may be considered as fixed. For a plasma with electron density n_e, the plasma frequency (ω_p) is given as [4],

$$\omega_p = \sqrt{\frac{n_e e^2}{\epsilon_0 m_e}} \tag{1.3}$$

where, m_e and e are the Mass and the charge of electron respectively.

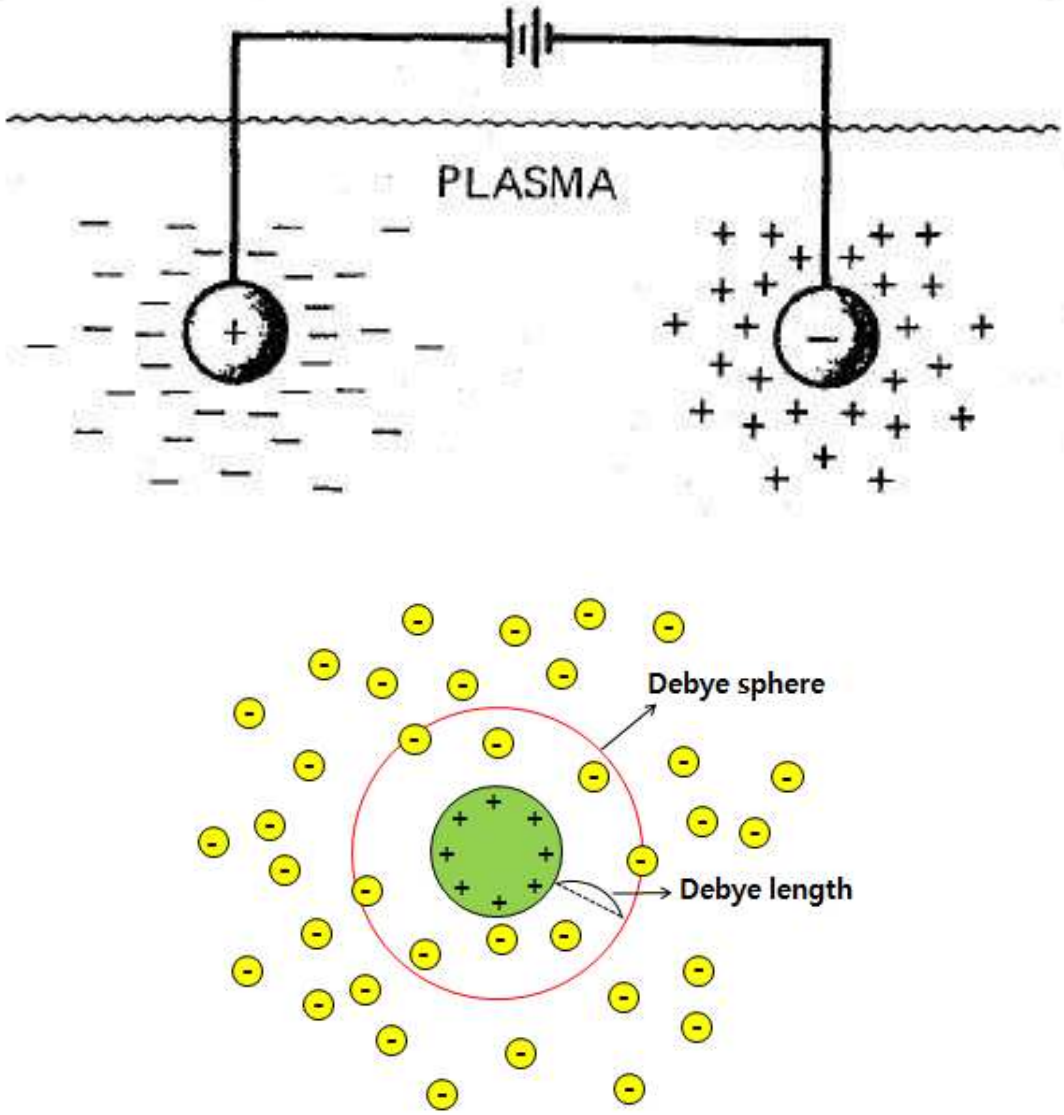

Figure 1.2: Debye shielding.

1.1.3 Criteria for plasma

Three fundamental parameters characterize a plasma:

- the particle density n (measured as particles per cubic meter),
- the temperature T of each species (usually measured in eV, where 1 eV=11,605 K),
- the steady state magnetic field B (measured in Tesla).
  A host of subsidiary parameters (e.g., Debye length, Larmor radius, plasma frequency, cyclotron frequency, thermal velocity) can be derived from these three fundamental parameters [1].

A host of subsidiary parameters (eg. Debye length,Larmour radius, plasma frequency,cyclotron frequency, thermal velocity) can be derived from these fundamental parameters [1]. The criteria for any ionized gas to be called plasma can be expressed in the following forms [4];

- Debye length is short compared to the physical size of plasma i.e. $\lambda_D \lll L$.
- There are large numbers of particles (ion or electron) within any Debye sphere i.e.$N_D \ggg 1$.
- Mean time between collisions of ions is usually long in comparison with the period of plasma oscillations i.e. $\omega\tau < 1$.

1.2 Thermonuclear Fusion

There are two schemes applied to harness nuclear energy; nuclear fusion and nuclear fission. In fission heavy nuclei are splitted into lighter nuclei having higher binding energy per nucleon, as the result there is release of energy. Nuclear fusion is a promising source of energy to support the growing world. Fusion energy power the sun and stars in which low- mass nuclei combine, or fuse, to form more massive nuclei nucleus having higher binding energy per nucleon. So there is also release of energy. A point to be noted here is that energy release

per nucleon in fusion is greater than that released in fission. The energy release per nucleon in fusion of two nuclei ${}_1H^2$ and ${}_1H^3$ is about 6 MeV per nucleon whereas in fission it is about 0.8 MeV per nucleon. In addition nuclear fuel that is used in fission is isotope ${}_{92}U^{235}$ and in fusion the fuel is deuterium, ${}_1H^2$. In naturally occurring Uranium, there is only 0.7% of ${}_{92}U^{235}$ whereas ${}_1H^2$ are abundantly found in nature. Hence, fusion has merit over fission [9].

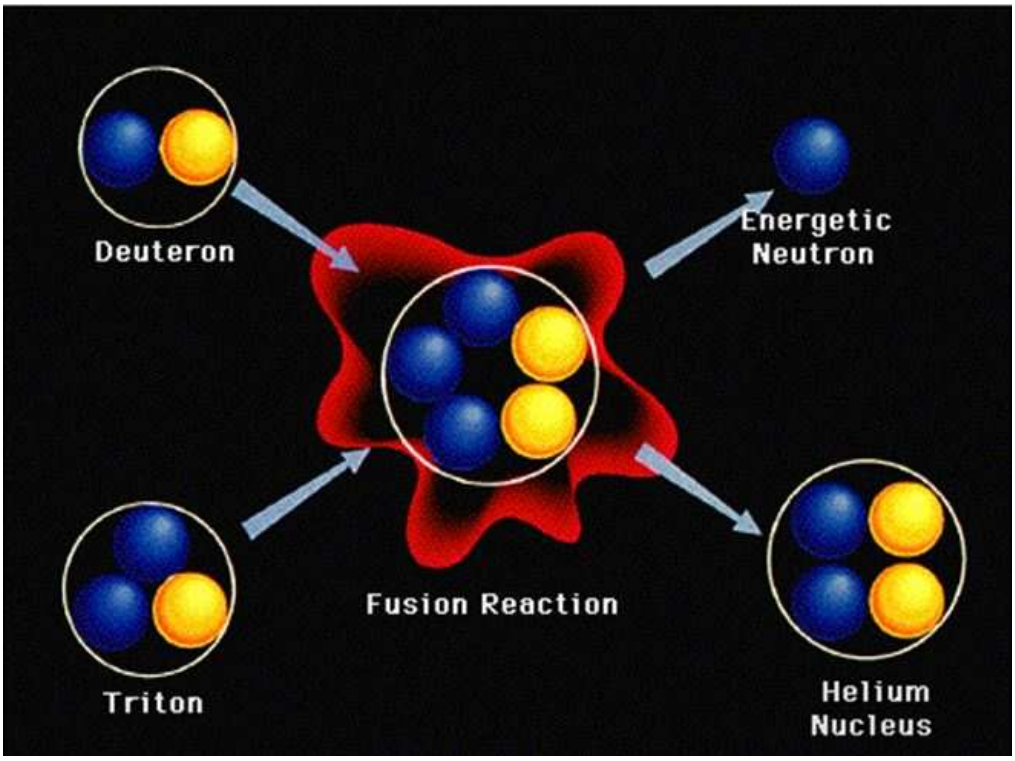

Figure 1.3: Deuterium-Tritium fusion reaction [9]

Fusion energy holds the promise of providing a significant part of the world's long term, environmentally acceptable energy supply. At the center of all schemes to make fusion energy is a plasma-an ionized gas that, like the center of the Sun, is heated by fusion reactions. A burning plasma experiment would address for the first time the scientific and technological questions that all magnetic fusion schemes must face [10]. Fusion power promises to be a safe, efficient and environmentally friendly energy source. Controlled fusion power concepts have been under investigation for decades.

A necessary but not sufficient condition for the achievement of a net release of energy from nuclear fusion reactions in a fusion reactor is formulated by Lawson, this condition simply stated that a minimum requirement for net energy release is that the fusion fuel charge must combust for at least enough time for the recovered fusion energy release to equal the sum of energy invested in heating that charge to fusion temperatures, plus other energy losses occurring during combustion [11]. The Lawson criterion is to be thought of as only a rule of thumb for measuring fusion progress; detailed evaluation of all energy dissipative and energy recovery processes is required in order properly to evaluate any specific system. Once a critical ignition temperature for nuclear fusion has been achieved, it must be maintained at that temperature for a long enough confinement time at a high enough ion density to obtain a net yield of energy. In 1957, Lawson showed that the product of ion density and confinement time determined the minimum conditions for productive fusion, and that product is commonly called Lawson's criterion. For D-T fuel, $n\tau > 10^{20} sm^{-3}$ at 10 keV temperature and for D-D fuel, $n\tau > 10^{23} sm^{-3}$ at 100 keV temperature. Where n is the plasma density, (τ) is confinement time. For an ignited fusion reactor, the triple product of plasma density (n), temperature (T) and the confinement time (τ) needs to exceed a critical value: $nT\tau = 3 \times 10^{21} m^{-3}$ keVs [12]. Nuclear fusion programmes take extraordinary amounts of combined international resources and cooperation on a scale never before attempted. Ongoing research on other devices such as pinches has shown that these are able to produce nuclear fusion even in devices of much smaller scales [13]. Such small scales experiments are suitable for research even by small groups in universities; yet these small scale experiments are able to demonstrate the potential for development of nuclear fusion energy. A superior method of producing super-dense and super-hot pinch is to use the Plasma Focus (PF) [14].

1.3 Dawning Towards Plasma Focus

When Christopher Columbus in 1492, sailed into the Americas the world consumption was less than 1% of the present day consumption with world population 450 million only. The world was highly populated. There were abundant energy resources waiting to be developed to support a larger and more progressive human civilization. In the past 100 years world population grew 4 times, whereas the energy consumption grew by 10 times. Which shows that the energy consumption per head grew by more than two times. It is well known fact that the per capita of energy is closely correlated with the standard of the living. In the past 100 years the population doubling time was 50 years whereas the consumption doubling time was 30 years. If this population were to be continue, world population would reach 27 billion in another 100 years on the other hand the energy consumption would increase by another 10 times. Energy used by today's industrial societies is derived from utilization of finite earth resources. Of course this is unsustainable condition as the world is already near to the critical situation where the supply of energy hardly meets the demand. The fossil fuel era is almost over [15].

As shown in the Figure 1.4, about 80 % of energy used on earth comes from fossil fuels: oil, gas and coal. It has been estimated that in 150 years about one half of the available resources will have been exploited. At the present rate of annual increase of energy use experts predicts that in about 30 years oil extraction will become inconvinient, whereas there should be about 2 centuries left for coal and natural gas should last 45-60 more years [11].

On the other hand if energy supplies were to become unlimited then there is no need to restrict the growth of energy consumption, a better standard of living or the growth of population. The following figure 1.5 clearly describes the energy consumption and the corresponding scenario into the 22^{nd} century. Which combines the existing projections of fossil, nuclear fission and renewable together with scenario of the development of the nuclear fusion. This is shows that it is possible to continue to grow the human civilization with the nuclear

fusion. The best practice of environmental conservatism could and should be incorporated into growth, so that efficient and 'green' habits become part of the sustained culture of the human race.

The scenario of Figure 1.6 below thus describes that the age of rapid growth of nuclear fusion will starts after the middle of this century. Fusion energy takes around half century to take up the slack and allow Mankind to Continue its progress and growth. Because the development of fusion energy is a complex technological task and also it demand more time and money. Fusion energy have more advantages over other form of energies like there is no risk of accidents as in the fission plants. It is the clean source of energy because there is no air pollution as well as no high level of nuclear waste and no generation of weapons materials like any radiations. Together with these the fuels is abundantly available and can be produced easily because fusion reactor is expected to use a mixture of deuterium and tritium as its first generation fuel.

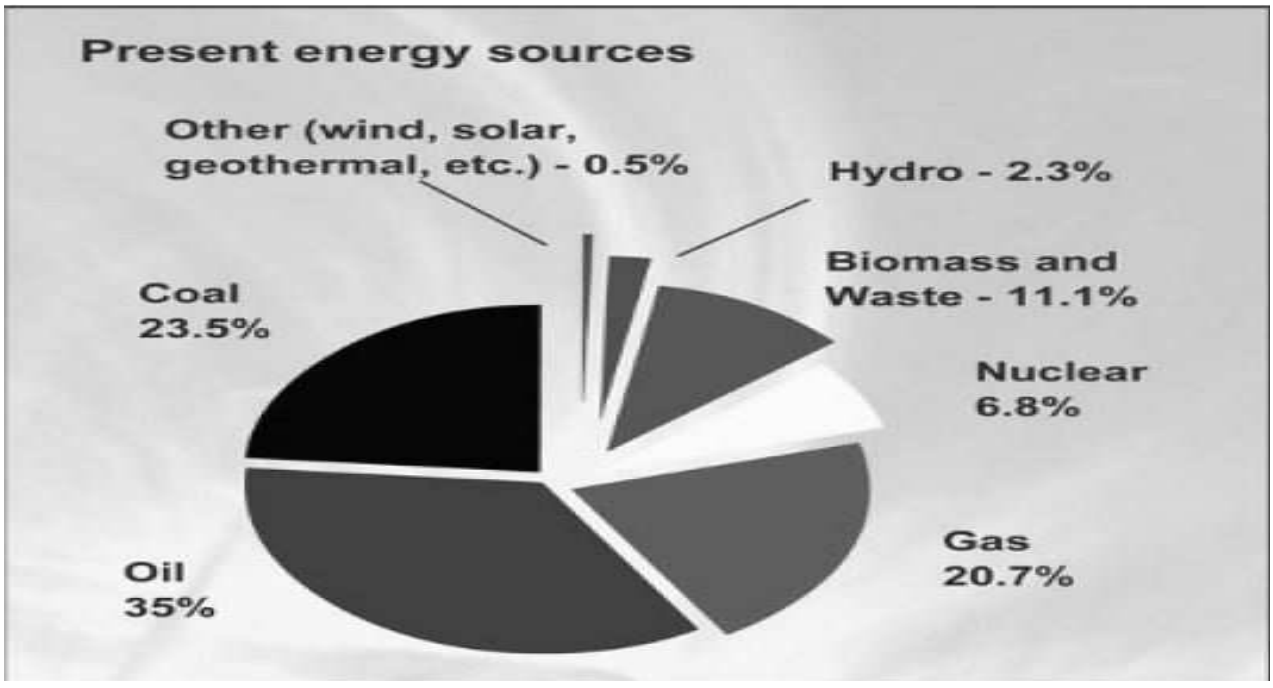

Figure 1.4: Energy sources. Most of the energy currently supplied to humanity comes from fossil fuels. Alternative sources provide about 20% of the energy used on earth [11].

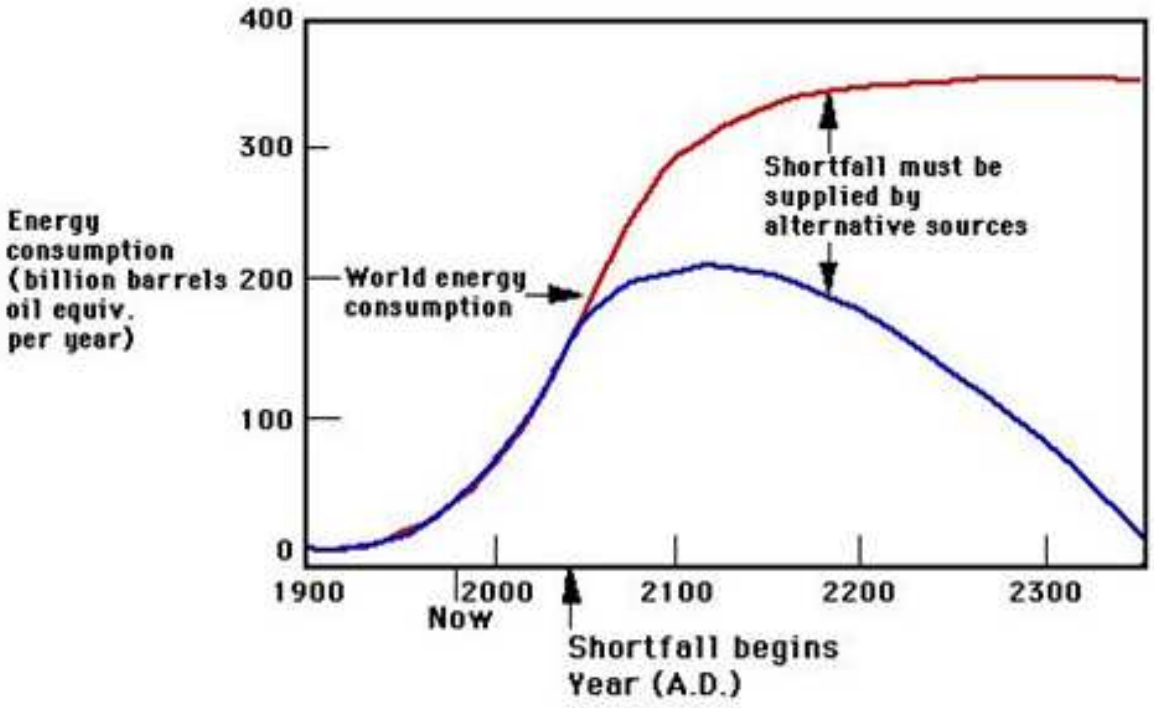

Figure 1.5: A scenario: Energy consumption based on a stabilized population of 10 billion with average energy consumption taken as $\frac{3}{4}$ of 1985 US per capita consumption [15].

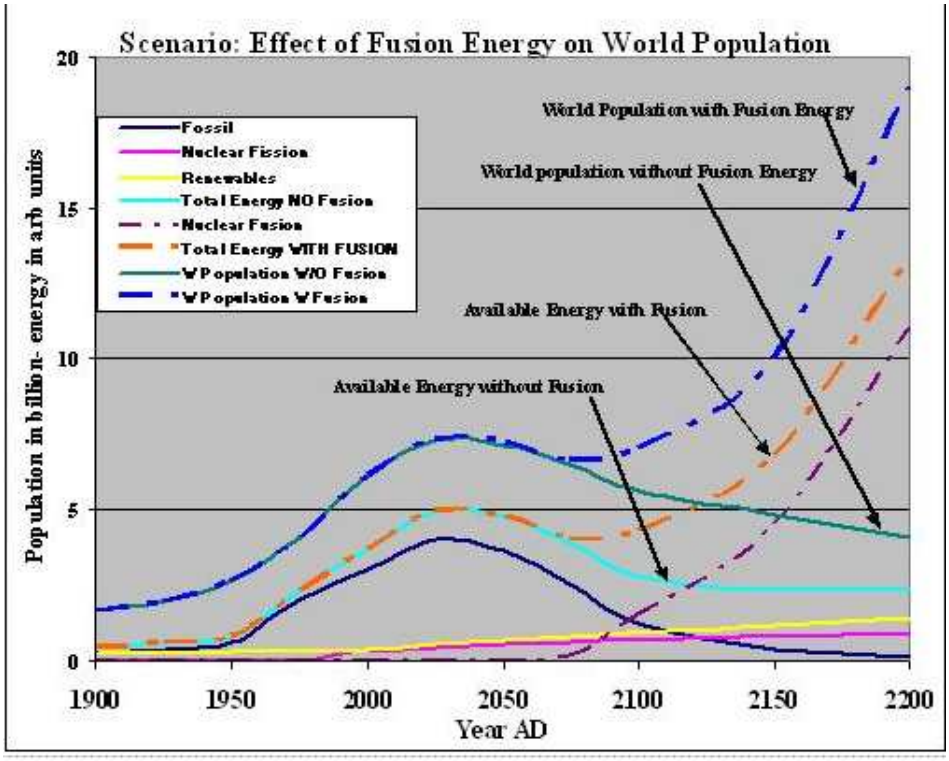

Figure 1.6: A scenario: Energy consumption based on continuing population growth; provided no limit to energy supply [15].

Man should have an unlimited destiny- to reach for the moon, as he already has; then to colonize it for its resources; likewise to reach for the planets and ultimately - the stars. Man's spirit must and will remain indomitable. The project is ITER-the International Thermonuclear Experimental Reactor which is currently being built in France at Cadarache. The process involves nuclear fusion which is the same process occurring in the stars causing their glow and powering all the energetics of the universe, including all life on earth. In the stanza below the dream (any dream), the river, the glamour and the night of the first two lines are all dependent on the process mentioned in the last two lines [15]:

And a dream lies on the river
And a glamour veils the night
Whilst above the white stars quiver
With nuclear fusion- bright

Nature thus showing the way, powering the whole universe with nuclear fusion. Einstein's $E = mc^2$ enabled to understand the energy and universe and Man will liberate his destiny with $E = mc^2$ in the nuclear fusion reactors [11].

Nuclear fusion is the process that powers the stars. The study of the plasma physics lead to the technological developments of new, clean and limitless energy source and In 1984 Rector Dr. Soedjatmoko of United Nations University (UNU) stated in a communication: "we have strong reasons to believe that plasma physics will be one of the major technologies of the future in developing as well as industrialized countries." Moreover the last final push is set to begin with an international consortium comprising the major economic and scientific communities of the world. There is a view that whereas Tokamaks and laser implosions will likely be the devices to succeed in the efforts to harness nuclear fusion [15]. An alternative method of producing a hot dense pinch is PF pinch which produces higher densities and temperature. PF is a machine that produces, a short-lived hot and dense plasma and can cause nuclear fusion and emit x-rays. PF has following advantages over other devices also shown in Table 1.1 [9]:

- Focus fusion reactors are safe and environmentally sound. No long-term radioactive by-products or pollutants are produced. The end-product is harmless helium gas.
- Focus fusion reactors are cheap. Almost all of the energy (98%) is released in the motion of charged particles that can be converted to electricity directly, thereby eliminating the need for generating steam to drive turbines, which account for most of the cost of electricity today. Focus fusion-generated electricity costs are projected to be as much as one hundred times less than present energy costs.
- Focus fusion reactors are small and decentralized. Focus fusion reactors can fit into a residential garage and can be made as small as 2 MW, sufficient for a small community.
- Focus fusion energy is essentially unlimited. The raw materials for hydrogen-boron fuel are exceedingly common and plentiful.

Table 1.1: Comparison of a Typical Plasma Focus Fusion Device with the Proposed Tokamak (ITER).

Reactor Type	**Plasma Focus Fusion**	**Tokamak**
Fuel	Hydrogen - Boron	Deuterium-tritium
Fuel availability	Abundantly available	Tritium must be bred
Long-lived radioactivity	None	Considerable
Radioactivity of structure	None	Considerable
Power output per unit	2 MW and up	500 MW and up
Unit size	$(3 \times 3 \times 9)$ feet	$(70 \times 70 \times 80)$ feet
Capital Cost per kW	(100 to 200) US dollar	(2000 to 3000) US dollar
Electricity conversion	Direct induction	Stream cycle

1.4 Plasma Focus as X-rays Emitter

X-rays are an indispensable part of modern technology. X-rays have become a most versatile tool for fundamental research and applications spanning physical, chemical and life sciences as well as materials technology, engineering and medicine. X-rays, including x-ray sources, their measurements and applications, have been extensively investigated. The stream of technological innovations using information derived from x-ray investigation includes semiconductor materials and devices, catalysts, magnetic storage media, drugs and enzyme analysis, micromachined components, chemical and mechanical sensors [16].

Common plasma sources, nowadays, are laser-generated plasmas (LGPs) and various types of pinch plasma. The most common type of pinch-plasma sources are the gas-puff z-pinch [17] and PF. PF is a special device for z-pinch and these are now widely studied as an effective x-ray source. The research topic of this thesis is the plasma dynamics and x-ray radiation properties of the PF [18].

For a long period after its discovery, the PF has been developed as a fusion device [9]. Which is extremely efficient device for compressing and heating plasmas in a pulsed mode. It is superior to the conventional Z-pinch in that it uses a pre-pinch phase to allow the capacitor current to reach a peak value before the pinch occurs. Thus the PF, using only a conventional capacitor, is able to produce a plasma of high density and temperature, superior to even the super-fast pinch, which requires an additional pulsed line to shape the capacitor discharge. Most of the studies being done in hydrogen or its isotopes, with minor attention paid to the x-ray emission. In a simple, cost effective manner, pinch plasmas are promising as emitters of soft x-ray pulses with duration from nanoseconds to hundreds of nanoseconds. The emission of x-rays from PF is characterized by high intensity and wide spectral range. The focus produces plasma electron density $n_e > 10^{20} cm^{-3}$ and temperature $T_e > 1keV$. The radiation spectrum in the x-ray region ranges from below 1 keV up to 500 keV. Emission times range from a few nanoseconds to a few hundred nanoseconds [19].

1.5 Merits of Plasma X-ray

The x-ray produced through PF is used in the diverse research field as discussed above. Moreover, we can list some of the merits of it over other.

- Duration of the x-ray pulse is in the order of few picosecond to nanosecond, which is very shorter than that of a conventional method of x- ray production.
- Emission spectrum can easily varied with a choice of target material. In case of the x-ray tube, only electrically conductive materials can be used as the anode.
- Source intensity is extremely bright in comparison with other sources.

On the other hand the most noticeable demerits of it is not a continuum spectral source [16].

1.6 Scope and Layout

This study is mainly intended for studying the emission characteristics of x-ray emission from a PF operated with neon using Lee Code and compare it with experimentally measured value. The work include:

1. The dependence of the x-ray emission on operating pressure.
2. Comparison of the total current wave-form of experimentally measured by using Lee Model Code and computed one.
3. Comparison of x-ray yield for measured value and computed one.

To study the gross dynamics of PF in neon, we use the Lee Model Code.

The dissertation work is organized as follows:

Chapter 1 (Introduction) describes the term plasma, fusion and PF together with the advantages of PF over fusion other devices.

Chapter 2 (Review of Plasma Focus) summarizes the previous studies in the field of the discovery and modification of PF with x-ray yield using PF.

Chapter 3 (Lee Code and Plasma Focus) generalizes the idea about the Lee Code and different phases of the PF.

Chapter 4 (Theoretical Model of Plasma Focus) presents the theoretical model for PF.

Chapter 5 (Results and Discussion) presents the experimental results obtained including the optimization condition for x-ray yield. It also contains discussion on the correlation between other pinch plasma dynamics and the gas pressure.

Chapter 6 (Conclusion and Future Works) contains the summary of the results and possible future work in this area.

Chapter 2

Review of Plasma Focus Studies

Studies on the confinement of plasma have always been a priority of interest for all practical plasma devices, specially for the magnetic confinement fusion device. Different attempt have been made to generalize the study of the confinement fusion. Among them PF is the most recent and effective device for producing the hot dense plasma and also used widely as an effective x-ray source. Following literature reviews are given on the dynamics of the PF and its application as an x-ray source.

The early work in USA with coaxial gun systems was pioneered by Marshall. Mather, following the work of Osher, investigated the fast coaxial gun mode which led to the development of the high pressure mode of operation. The PF device, in which an accelerated plasma is magnetically compressed to a short lived (50-200 ns), rather dense ($\sim 10^{-19}\ cm^{-3}$) and hot ($\sim$1keV) filament (focus), was discovered independently by Mather (USA) and Filippov (USSR) in early 1960s [20].

In the study of the x-ray emission the study of Liu is milestone, which leads the study in new age. It is clearly stated that the compression dynamics, discharge characteristics and the emission of radiation from 3 kJ PF on his Phd work. The strong correlation between neutron yield and the forwardly directed high energy deuteron beam emitted from the pinch region of PF was observed. Also there is a correlation between the emissions of neutrons, soft x-rays and hard x-rays with the electrical discharge parameters, characteristics time period and some of other important emission parameters of PF. At optimum condition (14 kV, 4 mbar) a total SXR yield of 6 J/shot at source into 4π steradians is observed from this plasma source. From the experiments listed on his work it seems that the discharge with longer pinch length appears to be more favorable for the soft x-ray production. On the other hand the neutron yield is lower, which help to conclude there is the close relationship between length of column and neutron production rather than the soft x-ray emission [18].

Lee's study (1984) is the milestone of the latest form of the Lee Model Code. As the very

first step he introduce the current-stepping technique and has been proposed as one of various means of producing a dense plasma [21]. It is stated that the proposed pinch fusion reactor concept fulfils the Lawson criterion and shown that the current step, switched on to the discharge current of a pinch as it approaches its quasi-equilibrium radius ratio. The paper shows successfully and present the current-stepping technique is able to significantly reduce the plasma pinch ratio and shows from the results that further enhancement of pinch compression by using multiple steps added to the primary pinching current.

According to Shan's study the x-ray emission properties of neon or argon plasma are dominated by the plasma temperature [16]. The optimized plasma temperature for generating neon or argon x-rays are $\sim$ 420eV and $\sim$ 3keV respectively. On the basis of the above fact it can be concluded that much higher energy is required to heat the argon plasma as compared to the neon plasma to suitable temperature, it means it is much easier to obtain soft x-rays from the neon PF. The thermodynamic properties such as ionization fraction and the specific heat ratios of the neon and argon on the context of the plasma dynamics and temperature are also compared. He also showed that the plasma dynamics in the radial inward shock phase plays an important role in determining the final plasma state and optimized working region for NX_2 is around 5.0 cm anode, $(2.0 - 2.5)$ mbar neon with 11.0 KV charging voltage. The x- ray yield is $\sim$ 12 Joule/shot at 5.0 Hz repetition rate.

Shahid (2002) developed and presented deails about the design, development and implementation of the three frame laser shadowgraphy system together with an automated deuteron energy spectra analysis system of a magnetic spectrometer. According to his work and claim the deuteron energy spectra were found in between 80 kev to 250 kev $80kev < E_d < 250keV$ with $100keV < E_d < 140keV$ the most frequent energy range for each pressure. Strong correlation between the neutron yield and the forwardly directed high energy deuteron beam emitted from the pinch region of PF was shown. The correlation is presented for all three pressures (3.5,4.0 and 4.5 mbar) and it was found that the neutron yield is higher for smaller

pinch and for the shorter pinch lifetime whereas the longer pinch length and longer pinch time favors the soft x-ray production. The column radius has more effect on the radiation emission compared to the pinch length. The radiation output (both the neutron yield and the soft x-ray) appears higher for the discharges with larger aspect ratio [20].

Lee and his group contributed in the development of the modified form of the numerical simulation package for PF device and have published large number of articles. They have developed the theory about the PF and presented the numerical simulation model. The radiation yield depends on

1. the absolute density
2. the temperature
3. the duration of the slow compression phase
4. the volume of the pinch plasma during the slow compression phase.

It is concluded that there is good agreement between the experimental and numerical experimental values and also shows neon soft x-ray yield for the NX_2 is a function of the pressure with reasonable degree of the agreement (In terms of absolute value of Y_{sxr} at optimum pressure as well as the optimum pressure itself) [22].

Lee et al carried out the numerical experiments systematically to determine the neon soft x-ray yield Y_{sxr} for optimized neon PF with storage energy E_0 from 0.2 kJ to 1 MJ and concluded for application requiring high x-ray yield, the PF have the design to optimize I_{pinch} and best fitted with $Y_{sxr} = 1.07 \times 10^{-7}\ (I_{pinch})^{3.63}$. On the basis result of series of the experiments the experimental yield enhancements are classified into three categories:

- compensating for unoptimized focus; where experiments start off with a focus showing unexpectedly low yield.
- Increasing I_{pinch}

- new regime of operation

where the plasma parameters such as density, dimensions and lifetime are changed at the same I_{pinch} and yield is beyond the scaling law [23].

Lee et al presented that the SXR pulses emitted from the INTI PF at 12 kV, 2 Torr neon are differentiated into the characteristic $He-like$ and $H-like$ neon line SXR with in the spectral window of $900-1550$ eV, and other neon SXR emission with photonic energy higher than 1550 eV and shows SXR emissions are carefully correlated to the time profiles of the measured and fitted computed currents. It was found that the characteristic $H-like$ or $He-like$ neon line SXR are emitted 10 ns before the pinch phase [24].

Rafique - et al (2010) developed the correlation between emission of neutrons and x-rays and the current sheath evolution during the radial phase of a 3.2 kJ Mather-type PF device operated in deuterium at the optimized pressure of 4 mbar. It is further concluded that x-rays and neutron emission characteristics enabled to identify the important regimes of the focus. That the focus operates in the two regimes namely known as;

- single compression regime
- multiple compression regime

The multiple compression region is indicative of the low radiation output, specially the neutron yield and hard x-rays as well as it is supportive to soft x-rays whereas the single compression regime is best suited for the high neutron yield and hard x-rays output. The correlation with the high voltage probe signal of the discharge, together with the x-ray and neutron emission regimes enabled to identify the important periods of the evolution [25]

Saw et al stated by shortening the anode length z_0 from the initial, z_0 16 cm to 7 cm together with increasing the length of the anode used in the plasma device from 0.95 cm to 1.2 cm, the optimum yield of Y_{sxr} was achieved, where the Y_{sxr} have the value 9.5 Joule

with other parameter of the device remaining constant where the cathode length is taken as normal length and is taken as 3.2 cm. For the operation of the neon it was considered that the focus temperature between 200 and 500 eV. The anode length was reduced in order to maintain time matching [26].

Akel et al listed oxygen parameter at different temperatures by calculation and the emission properties of oxygen plasma were investigated with the help of the Corona model. In turns the Lee Model Code $RADPF5.15a$ was modified to get $RADPF5.15K$ including oxygen gas and which is used to characterize the Rico PF (1kJ) using its experimental parameter, by changing pressure $P_0 = 0.2Torr$ to 0.745 Torr the Y_{sxr} will increase to 6.8 mJ which is the optimum value for RPF(1 kJ). That the modified Lee Model code was also used to run numerical experiments on $PF - SY2$ with oxygen gas for optimizing soft x-ray yield with reducing L_0, varying z_0 and a [27].

Akel et al carried out the numerical experiments systematically to determine the nitrogen x-ray yield. In this work the Lee Model Code RADPF5.15a was modified to $PF - SY1$ and it was concluded that plasma temperature for nitrogen x-ray output is to be around 160 eV with the maximum x-ray yield 64 mJ. The bank parameters and the tube voltage are kept unchanged with p_0 =0.09 Torr, $z_0 = 7.2$ cm and $a = 2.58$ cm [28].

Mohammadi et al investigated through the series of the experiments on the x-ray emission characteristics of a neon filled $UNU - ICTP$ PF device with the effect of three different anode shapes, flat, tapered and hemispherical. They claim that the maximum neon soft x-ray (SXR) yield for flat anode is about (7.5 ± 0.4) J at 4 mbar, whereas for tapered anode and hemispherical anode are almost half i.e., (4.0 ± 0.3) J and (3.3 ± 0.2) J respectively at 3 mbar and the relative HXR yield claimed was for the hemispherical anode followed by the tapered and the flat anodes in that order. It was concluded that for the hemispherical anode the multiple- pinch phenomenon was most commonly observed which could be responsible

for multiple HXR bursts for this anode with maximum HXR yields [29].

Patran presented an investigation of electron and x-ray emission from a 3 kJ PF operated with neon gas. Derivative Rogowski coils, high voltage dividers, minimum radius detector, CCD camera, soft x-ray spectrometer of range 0.5 to 40 keV, Scintillator photomultiplier detector for x-rays above 70 keV and electron energy analyzer for the range 30 to 660 keV are the diagnostic techniques used over his study. By developing a computer simulation program for charged particle trajectories in non-constant magnetic field this study help for further improvement of Lee Model Code. During his work the charging voltage was 14 keV with the operating pressure in the range 1.5 to 5.5 mbar. On his study he showed electron emission above 350 keV is negligible and on the other hand discharge featuring electron emission concentrated below 200 keV using NIE-NSAG-PFF device. The strong correlation between the electron current emission and the x-ray photons in range of 20 keV to 40 KeV was observed. This is because of the reason that the origin of both these phenomena is the electron emission from a turbulent plasma [30].

Saw investigated experimentally the effect of a current step on the enhancement of pinch compression predicted by the theory of energy balance. It was proved from that the assumptions of a plasma of infinite conductivity in the energy balance slug model together with a constant specific heat ratio, γ equals to 5/3 at the moment of current stepping are not valid in the experiment. The energy balance slug model is extended to represent more closely the real plasma condition with transient effective specific heat ratio, γ_{eff}. The electrical signals of the plasma current and voltage and streak photographs of the radial compression were taken of the z-pinch plasma without and with current stepping. In this work the energy balance slug model was incorporated in UMCSZP and a new system MLCCSZP was designed [31].

Chapter 3

Plasma Focus and Lee Model Code

3.1 Dense Plasma Focus and Lee Model Code

A dense plasma focus (DPF) is a machine that produces, by electromagnetic acceleration and compression, a short-lived hot and dense plasma and can cause nuclear fusion and emit x-rays. The electromagnetic compression of the plasma is called a pinch. It was invented in the early 1960s by Mather and also independently by Filippov in 1954 [20]. PF is similar to the high-intensity plasma gun device (HIPGD) (or just plasma gun), which ejects plasma in the form of a plasmoid, without pinching it [32]. Moreover a compact powerful pulsed sources of radiation known as PF. During the intense burst of radiation, extremely high powers are achieved. For example the x-ray emission peaks at 109 W over a period of nanoseconds. The emission comes from a point source making these devices among the most powerful laboratory pulsed radiation sources in the world. These sources are plasma-based. An alternative method of producing the super-dense and super-hot pinch is to use the PF. Not only does this device produce superior densities and temperatures, moreover its method of operation does away with the extra layer of technology required by the expensive and inefficient pulse-shaping line. A simple capacitor discharge is sufficient to power the PF.

The schematic arrangement of PF electrodes system and the diagnostics is shown in figure 3.1. The experiment is conducted on a PF system energized by a 32 μF single capacitor with charging voltage 12 kV (2.3 kJ) giving a peak discharge current of about 190 kA and the parasitic inductance of the system is supposed to be 80 nH. The anode is a Cu electrode of diameter 18 mm with length 160 mm (measured from the cathode base plate) and the cathode rods are screwed to a Cu plate, called the cathode base plate [33].

Figure 3.2 shows the schematic diagram for DPF and shows simple capacitor discharge is sufficient to power PF. The working of PF device is divided into two sections. The first is a pre-pinch (axial) section. The function of this section is primarily to delay the pinch until the capacitor discharge (rising in a sinusoidal fashion) approaches its maximum current. This

is done by driving a current sheet down an axial (acceleration) section until the capacitor current approaches its peak. Then the current sheet is allowed to transition into a radial compression phase. Thus the pinch starts and occurs at the top of the current pulse. This is equivalent to driving the pinch with a super-fast rising current; without necessitating the fast line technology. Moreover the intensity which is achieved is superior to the line driven pinch. Figure 3.3 shows the shadowgraphs of the PF pinching process. The shadowgraphs are taken at different times. The times indicates in the shadowgraphs are relative to moment of maximum compression. That moment is taken as t = 0 ns. The quality of the plasma compression can be seen to be very good, with excellent axisymmetry, and a very well compressed dense plasma.

Lee's study at 1984 is the first step and is the milestone of the latest form of the Lee Model Code. As at 1984 he introduce the current-stepping technique and proposed as one of the various means of producing a dense plasma [21] and at 1985 Ali formulated the numerical model [31]. Lee organized a network of ten identical DPF machines operates in eight countries around the world in 1986 and is well known by the name AAAPT (Asian African Association

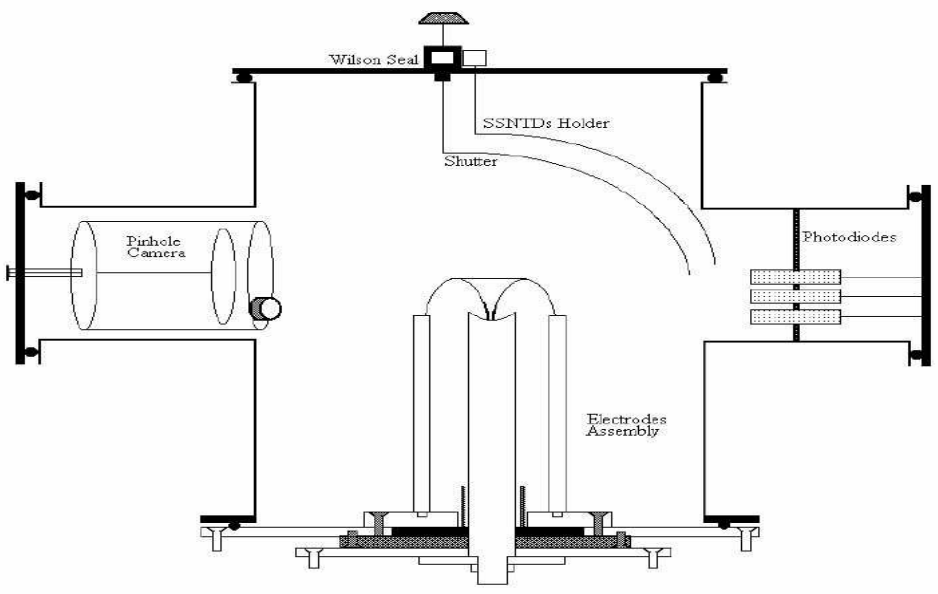

Figure 3.1: *Schematic arrangement of plasma focus electrodes system and diagnostics [33].*

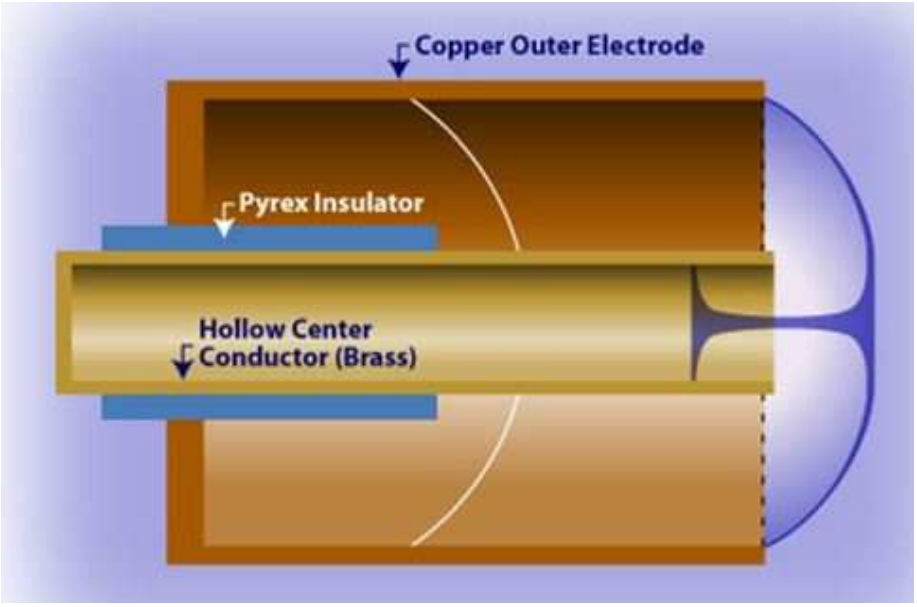

Figure 3.2: Dense plasma focus device. Image from [33]

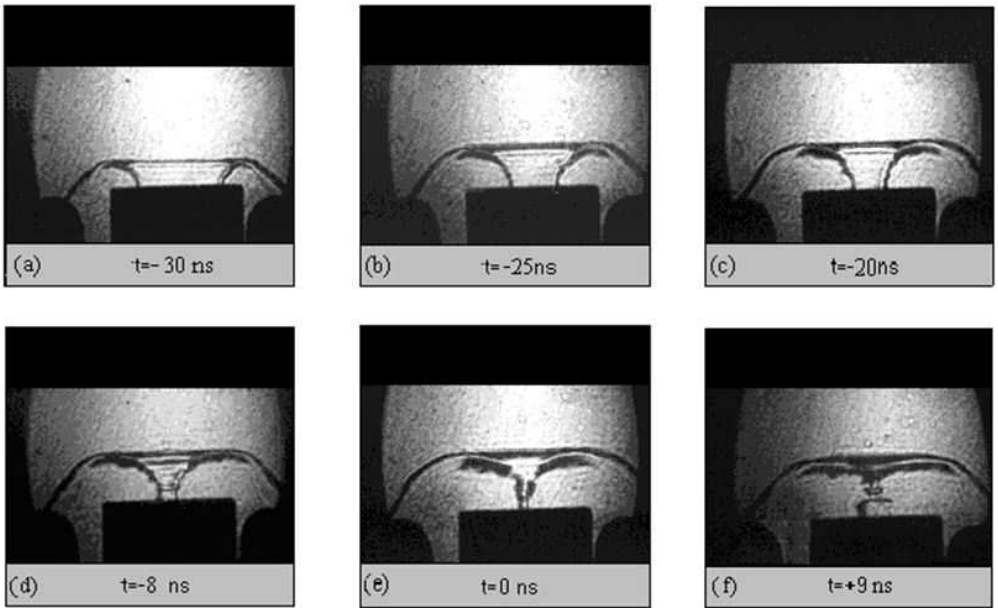

Figure 3.3: Shadowgraphic sequence showing formation of the plasma focus pinch. Sequential images from (a) to (d) show the plasma column being 'pinched' radially inwards; (e) being the time of maximum compression forming the hot and dense 'fusioning' plasma image from [33].

for Plasma Training). This network generally produces research paper on the topic and the optimization, diagnostics (neutrons, electron, soft x-ray and ion beams). This network also produces the research paper on applications (microlithography, micromachining, materials modification and fabrication, imaging and medical, astrophysical simulation) as well as modeling and computation. A simulation package, The Lee Model Code has been developed for this network. This model code couples the electrical circuit with PF dynamics, thermodynamics and radiation, enabling realistic simulation of all focus properties. The basic model described in 1984 [34] was successfully used to assist several projects. Radiation-coupled dynamics was included in the five-phase code leading to numerical experiments on radiation cooling. The vital role of a finite small disturbance speed discussed by Potter in a Z-pinch situation was incorporated together with real gas thermodynamics and radiation-yield terms.

Before this 'communication delay effect' was incorporated, the model consistently overestimated the radial speeds. This is serious from the point of view of neutron yields. A factor of 2 in shock speeds gives a factor of 4 in temperatures leading to a difference in fusion cross-sections of 1000 at the range of temperatures we are dealing with Plasma self-absorption was included in 2007 improving SXR yield simulation. The code has been used extensively for all of the PF devices including UNU/ICTP PFF, NX2, NX1, and adapted for the Filippov-type PF DENA [32]. This Model Code typically creates the excellent agreement between the real experimentally measured results and the computed results. The institute for Plasma Focus Studies (IPFS) was founded on 25 February 2008 to promote the use of Lee Model Code and encourage the application of PF numerical experiments.

Systamatically the whole process are divided into five phases. These five phases and the code are described as [22, 26]:

3.1.1 Axial phase

The equation of motion described by a snowplow model coupled to a circuit equation. The equation of motion incorporates the axial phase model parameters: mass and current factors f_m and f_c. Where the mass swept-up factor f_m accounts for not only the porosity of the current sheet but also for the inclination of the moving current sheet- shock front structure and all other unspecified effects which have effects equivalent to increasing or reducing the amount of mass in the moving structure, during the axial phase. The current factor, f_c, accounts for the fraction of current effectively flowing in the moving structure. This defines the fraction of current effectively driving the structure, during the axial phase.

3.1.2 Radial inward shock phase

Described by 4 coupled equations using an elongating slug model. The first equation computes the radial inward shock speed from the driving magnetic pressure. The second equation computes the axial elongation speed of the column. The third equation computes the speed of the current sheath, also called the magnetic piston, allowing the current sheath to sepa-

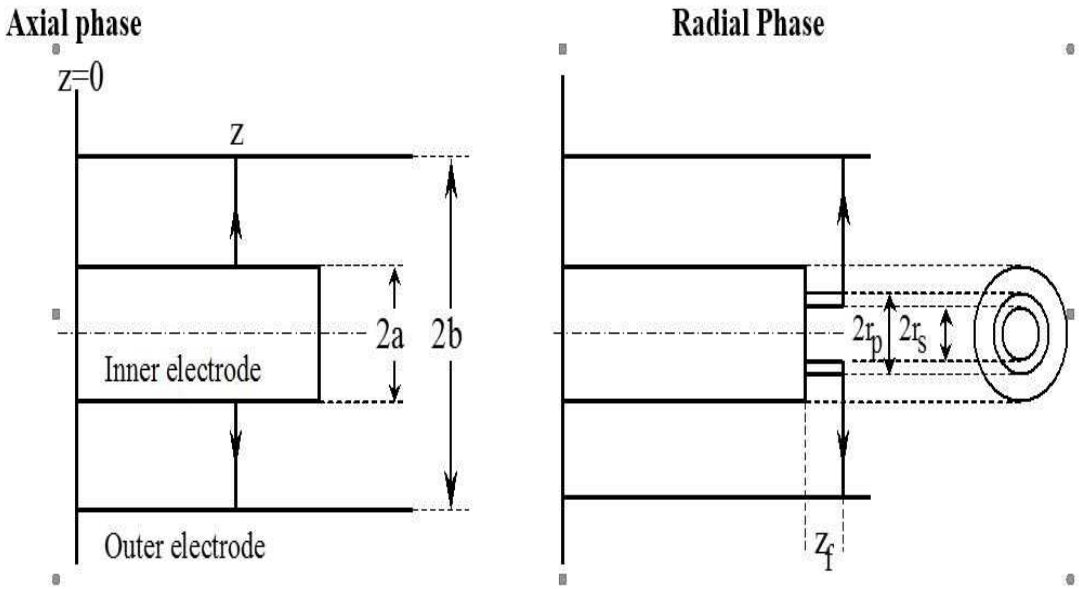

Figure 3.4: Illustrating the two phases of a Plasma Focus [33]

rate from the shock front by applying an adiabatic approximation. The fourth is the circuit equation. Thermodynamic effects due to ionization and excitation are incorporated into these equations, these effects being important for gases other than hydrogen and deuterium. Temperature and number densities are computed during this phase. A communication delay between shock front and current sheath due to the finite small disturbance speed is crucially implemented in this phase. The model parameters, radial phase mass swept-up and current factors, f_{mr} and f_{cr}, are incorporated in all three radial phases. The mass swept-up factor f_{mr} accounts for all mechanisms which have effects equivalent to increasing or reducing the amount of mass in the moving slug, during the radial phase. The current factor, f_{cr}, accounts for the fraction of current effectively flowing in the moving piston forming the back of the slug (due to all effects). This defines the fraction of current effectively driving the radial slug.

3.1.3 Radial reflected shock phase

When the shock front hits the axis, because the focus plasma is collisional, a reflected shock develops which moves radially outwards, whilst the radial current sheath piston continues to move inwards. Four coupled equations are also used to describe this phase, these being for the reflected shock moving radially outwards, the piston moving radially inwards, the elongation of the annular column and the circuit. The same model parameters, f_{mr} and f_{cr}, are used as in the previous radial phase. The plasma temperature behind the reflected shock undergoes a jump by a factor ~ 2.

3.1.4 Slow compression (Quiescent) or pinch phase

When the out-going reflected shock hits the in-going piston the compression enters a radiative phase in which for gases such as neon, radiation emission may actually enhance the compression where we have included energy loss/gain terms from Joule heating and radiation losses into the piston equation of motion. Three coupled equations describe this phase; these being the piston radial motion equation, the pinch column elongation equation and the circuit equation, incorporating the same model parameters as in the previous two phases. Ther-

modynamic effects are incorporated into this phase. The duration of this slow compression phase is set as the time of transit of small disturbances across the pinched plasma column. The computation of this phase is terminated at the end of this duration.

3.1.5 Expanded column phase

To simulate the current trace beyond this point, we allow the column to suddenly attain the radius of the anode, and use the expanded column inductance for further integration. In this final phase the snowplow model is used, and two coupled equations are used; similar to the axial phase above. This phase is not considered important as it occurs after the focus pinch.

It is noted that the transition from Phase 4 to Phase 5 is observed in laboratory measurements to occur in an extremely short time with plasma current disruptions resulting in localized regions of high densities and temperatures. These localized regions are not modeled in the code, which consequently computes only an average uniform density, and an average uniform temperature which are considerably lower than measured peak density and temperature. However, because the 4 model parameters are obtained by fitting the computed total current waveform to the measured total current waveform, the model incorporates the energy and mass balances equivalent, at least in the gross sense, to all the processes which are not even specifically modeled. Hence the computed gross features such as speeds and trajectories and integrated soft x-ray yields have been extensively tested in numerical experiments for several machines and are found to be comparable with measured values [22, 35].

Chapter 4

Theoretical Model of Plasma Focus

4.1 Description of Model

The latest form of the PF is the modified form of the device given originally by Mather. For the purpose of developing and implementing the computational model, the evolution processes were simplified as shown in the figure 4.1. This approach is based on the works of Lee and Liu [20]. Those processes are treated as four phases in the modeling (axial phase and three phases in the radial phase). Expanded column axial phase is added to 4-phase

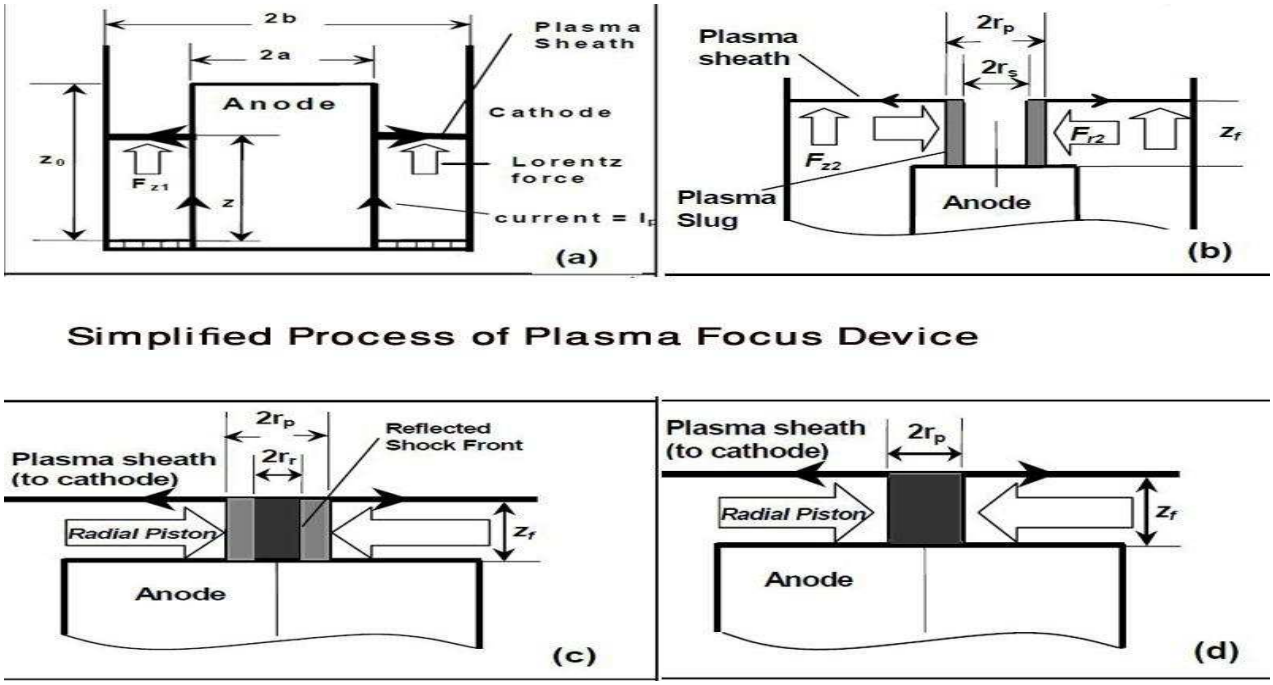

Figure 4.1: *Simplified Process [20].*

model to make the latest form of the model. That's why the latest form of model is known as 5-phase model. These are listed and described in detail in the following section:

1. Axial Phase
2. Radial Inward Shock Phase
3. Radial Reflected Shock Phase

4. Slow Compression (Radiative) Phase

5. Expanded Column Axial Phase

4.2 Axial Phase

4.2.1 Equation of motion(Snow-Plow model)

For the axial phase according a simple one dimensional Snow - Plow model coupled to a circuit equation is adequate to a circuit equation is adequate to describe the relationship between the plasma trajectory and the driving current. In this model all the mass encountered by the current sheet in its motion from $z = 0$ to position z has been swept up, and at time to all this mass $\rho_0\pi(b^2 - a^2)z$ is gathered at the position z leaving a vacuum between z_0 and z ahead of z gas is undisturbed [36]. As,

$$m = \rho_0 V = \pi\rho_0 z \int_a^b (rdr) = \pi\rho_0(b^2 - a^2)z \tag{4.1}$$

Then,

$$\frac{d}{dt}(mv) = \frac{d}{dt}[(\pi\rho_0(b^2 - a^2)f_m\frac{dz}{dt}] \tag{4.2}$$

$$F = \frac{d}{dt}(mv) = \pi\rho_0(c^2 - 1)a^2 f_m \frac{d}{dt}(z\frac{dz}{dt}) \tag{4.3}$$

where, f_m is the fraction of the mass swept down the tube in the axial direction with $f_m < 1$. Again the magnetic force on the current sheath is,

$$B = \frac{\mu_0 I}{2(\pi)r} f_c \tag{4.4}$$

where, f_c is the fraction of the current flowing in the piston.

Here, the magnetic pressure $= \frac{B^2}{2\mu_0}$

Now,

$$F = \int_a^b \frac{B^2}{2\mu_0} \times 2(\pi)r \tag{4.5}$$

[As we have $F = P \times A$]

On solving with substituting the value of B. We will have,

$$F = \frac{I^2 \mu_0}{4\pi} f_c^2 (\ln(c)) \tag{4.6}$$

Solving with the help of the equations $(4.3) and (4.6)$ we get,

$$\frac{d^2 z}{dt^2} = [\frac{f_c^2}{f_m} \frac{\mu_0^2 (ln(c))}{4(\pi^2)\rho_0 (c^2 - 1)} (\frac{I}{a})^2 - (\frac{dz}{dt})^2]/z \tag{4.7}$$

4.2.2 Circuit (Current) equation:

The energy bank is initially charged to a high voltage V_0 [20]. According to Krichoff's Law, the equation of the above circuit can be written as,

$$\frac{1}{c_0} \int_0^t I dt - V_0 + r_0 I + \frac{d}{dt}(L_0 I) + r_p I_p + \frac{d}{dt}(L_p I_p) = 0 \tag{4.8}$$

where, r_p is the plasma resistance with the variation of time which is ignored. Which is the approximation and generally used for the electromagnetic drive [37]. Then the above equation becomes as,

$$\frac{1}{c_0} \int_0^t I dt - V_0 + r_0 I + \frac{d}{dt}(L_0 I) + \frac{d}{dt}(L_p I_p) = 0 \tag{4.9}$$

The induced magnetic field between the electrode is,

$$B_\theta = \frac{(\mu_0) I_p}{2(\pi) r} \tag{4.10}$$

where, $I_p = f_c I$ is the current flowing through the plasma and f_c is a current shedding factor which is defined above.

The resultant $\overrightarrow{J} \times \overrightarrow{B}$ force on the plasma sheath is directed axially upward to the open end of the anode. The force exerted by the magnetic piston to drive the plasma sheath can be expressed as [20],

$$F_(z_1) = \int_a^b I_p \frac{(\mu_0) I_p}{2(\pi) r} dr = \frac{(\mu_0)(I_p)^2}{2(\pi)} \ln(c) \tag{4.11}$$

The inductance is,

$$L_{(}p_1) = \frac{\mu_0}{2\pi} z \ln(c) \tag{4.12}$$

From the equation (4.9) we get on substituting the value of the inductance and the plasma current.

$$\frac{1}{c_0}\int_0^t I dt - V_0 + r_0 I + L_0 \frac{d}{dt}(I) + \frac{d}{dt}(\frac{\mu_0}{2\pi} z I f_c \ln(c)) = 0 \tag{4.13}$$

Then,

$$\frac{dI}{dt} = [V_0 - \frac{1}{c_0}\int_0^t I dt - r_0 I - \frac{\mu_0}{2\pi} I f_c \ln(c)\frac{dz}{dt}]/[L_0 + \frac{\mu_0}{2\pi} z f_c \ln(c)] \tag{4.14}$$

Equations (4.7)and(4.14) are the generating equations of the model. These equation contain the physics built into the model and are the coupled equations. The equation of the motion (4.7) is affected by the electric current and the circuit equation (4.14) is affected by the current sheath motion $\frac{dz}{dt}$ and position z.

Normalizing the above equations(4.7) and (4.14) with replacing variables t, z and I by non-dimensionalised quantities as: $\tau = \frac{t}{t_0}$, $\zeta = \frac{z}{z_0}$, $\iota = \frac{I}{I_0}$, where $I_0 = \frac{V_0}{Z_0}$, ($Z_0 = \sqrt{\frac{L_0}{C_0}}$ is the surge impedance along with I_0 as peak current of the $L_0 - C_0$ discharge circuit with the capacitor C_0 charged initially to V_0), z_0 is the anode length and $t_0 = \sqrt{L_0 C_0}$ are the normalizing quantities and must be chosen carefully [37, 38].

Now, the equation of the motion becomes as:

$$\frac{d^2\zeta}{d\tau^2} = [\frac{f_c^2}{f_m}\frac{\mu_0^2(ln(c))}{4(\pi^2)\rho_0(c^2-1)}(\frac{I_0}{a})^2(\frac{{t_0}^2}{{z_0}^2})\tau^2 - (\frac{d\zeta}{d\tau})^2]/\zeta \tag{4.15}$$

Which we can write as

$$\frac{d^2\zeta}{d\tau^2} = \frac{[\alpha^2 t^2 - (\frac{d\zeta}{d\tau})^2]}{\zeta} \tag{4.16}$$

where, α is the scaling parameter and from the inspection of equation number (4.16) it is dimensionless and is,

$$\alpha^2 = {t_0}^2/[[\frac{{z_0}^2}{(\frac{I_0}{a})^2}](\frac{f_m}{f_c})^2[\frac{4(\pi^2)\rho_0(c^2-1)}{\mu_0^2(ln(c))}]] \tag{4.17}$$

Here, t_0 is the time value so has the dimension of time and we may define the denominator as the square of new time value denoted by t_a and is characteristic axial time of the current sheath (CS) down the anode axial phase. Then we can write α as the ratio of the characteristic discharge time to the characteristic axial time (i.e. $\alpha = (\frac{t_0}{t_a})$. For calculating the value of the characteristic axial speed we can use $V_a = \frac{z_0}{t_a}$.

Again, normalizing the circuit (current) Equation, we have:

$$\frac{d\iota}{d\tau} = [1 - \int \iota d\tau - f_c[\frac{\frac{\mu_0}{2\pi}(\ln(c))z_0}{L_0} - (\frac{r_0}{Z_0})]\iota\frac{d\zeta}{d\tau}]/[1 + f_c\frac{[\frac{\mu_0}{2\pi}(\ln(c))z_0]\zeta}{L_0}] \tag{4.18}$$

Now, this equation(4.18) becomes:

$$\frac{d\iota}{d\tau} = \frac{[1 - \int \iota d\tau - \beta\iota\frac{d\zeta}{d\tau} - \delta\iota]}{[1 + \beta\zeta]} \tag{4.19}$$

where, β is the second scaling parameter and is defined as the ratio of load to source inductance (i.e. $\beta = \frac{L_a}{L_0}$) and the device is electromagnetic, the electro-magnetics is determined by this scaling parameter, it is noted that $L_a = \frac{f_c\mu_0}{2\pi}\ln(c)z_0$ is the inductance of the axial phase when current sheath reaches the end $z = z_0$ and $\delta(= \frac{r_0}{Z_0})$ is the ratio of the circuit stray resistance to surge impedance and known as the third scaling parameter. This acts as a damping effect on the current [39].

Equations (4.16) and (4.19) are the generating equations that may be integrated step by step to calculate the unknown variables in the equation above [37].

Step for Calculating voltage across input terminals of the focus tube:

The voltage across the input terminals $(V) = \frac{d}{dt}(LI_pf_c)$

On substituting the value of $I_p(= If_c)$ and solving the equation.

$$V = f_cI\frac{L}{dt} + f_cL\frac{dI}{dt} \tag{4.20}$$

where, $L(= \frac{\mu_0}{2\pi}(l_nc)$

The normalizing form of the voltage becomes as,

$$\nu = \frac{V}{V_0} \tag{4.21}$$

Integrating, the above equation with initial condition:
$\tau = 0, \frac{d\zeta}{d\tau} = 0, \zeta = 0, \iota = 0, \int \iota d\tau = 0, \frac{d\iota}{d\tau} = 1, \frac{d^2\zeta}{d\tau^2} = \alpha\sqrt{\frac{2}{3}}$
Also setting the time of increment as D = 0.001 and the time after increment becomes as, $\tau = \tau + D$ [36]. Next step value are computed using the method of the linear approximations. That enable us to compute the new generating values of the circuit equation and the equation of motion using generating equations (4.16) and (4.19).

The above process repeated until $\zeta = 1$. Now the axial phase completed and then radial inward shock phase started [37, 39].

4.3 Radial Phase

At the end of the axial rundown phase, the current sheath sweeps around the end of the inner electrode (usually anode) and finally collapses due to inward $\overrightarrow{J} \times \overrightarrow{B}$ force. This collapse occurs within $50 - 200$ ns depending on the device characteristics. The collapse velocities range between 7 and 60 $cm/\mu_0 s$ depending on the geometry of the electrode, initial gas pressure, structure of the current sheath and electrical characteristics of the device.

This phase is important due to its extremely high energy density, transient character, the emission of intense radiation, high energy particles and for copious nuclear fusion products as well, when operated in deuterium of D-T mixtures.

The radial phase can be subdivided into four subspaces, namely Radial Inward Shock Phase, Radial Reflected Shock Phase, Slow Compression (Radiative) Phase, Expanded Column Axial Phase. In the following sub-sections of radial phases are discussed in detail [40].

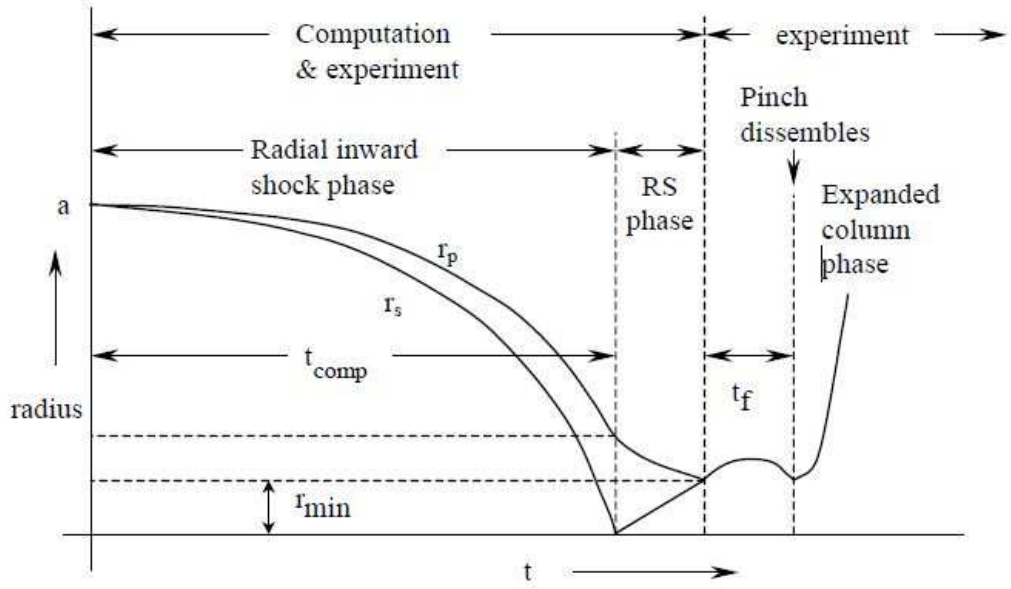

Figure 4.2: *Schematic of radius vs time trajectories to illustrate the radial inward shock phase when rs moves radially inwards, the reflected shock (RS) phase when the reflected shock moves radially outwards, until it hits the incoming piston rp leading to the start of the pinch phase (tf) and finally the expanded column phase [33].*

4.3.1 Radial inward shock phase

The snowplow model is used for axial phase just to obtain reasonable current profile. As the CS is assumed to be infinitesimally thin, no information of density is contained in the physics of the equation of motion, although an estimate of density may be obtained by invoking additional mechanics (eg. using shock wave theory) [41].

In the radial phase however, a snowplow model would eventually lead to all current flowing at a = 0, with infinite inductance and density.

We thus replace the snow-plow model by a slug model. In this model the magnetic pressure drives a shock wave ahead of it, creating a space for the magnetic piston (CS) to move into.

The speed of the inward radial shock front (see fig.4.1) is determined by the magnetic pressure. The speed of the magnetic piston is determined by the first law of thermodynamics applied to the effective increase in volume between SF and CS created by the incremental motion of the SF.

The compression is treated as an elongating pinch. Four generating equation are needed to describe the motion of (a) SF (b) CS (c) pinch elongation and (d)the electric current; to integrate for the four variables r_s, r_p, z_f and I.

Motion of shock front

From shock wave theory, shock pressure

$$P = \frac{2}{\gamma + 1}\rho_0 \upsilon_s^2 \tag{4.22}$$

where shock speed υ_s into ambient gas ρ_0 causes the pressure of the shocked gas to rise to value P.

If we assume that this pressure is uniform from the SF to CS then across the piston, we may

apply

$$P = P_m \tag{4.23}$$

where, $P_m = \frac{(\frac{\mu_0 I f_c}{2\pi r_p})^2}{2\mu_0}$

Thus,

$$\upsilon_s^2 = \frac{\mu_0 (I f_c)^2}{8\pi^2 r_p} \frac{\gamma + 1}{2\rho_0 f_{mr}} \tag{4.24}$$

where, f_c is same as in the axial phase and $\rho_0 f_{mr}$ is the effective mass density swept into the radial slug; where f_{mr} is a different (generally larger) factor than f_m of the axial phase.

Thus

$$\frac{dr_s}{dt} = \sqrt{\frac{\mu_0 \gamma + 1}{\rho_0}} \frac{f_c}{\sqrt{f_{mr}}} \frac{I}{4\pi r_p} \tag{4.25}$$

Which gives the motion of shock front [37, 39].

Elongation speed of CS(open- ended at both ends)

The radial compression is open at one end. Hence an axial shock is propagated in the Z-direction, towards the downstream anode axis. We take z_f as the position of the axial CS. The pressure driving the axial shock is same as the pressure driving the inward radial shock. The CS speed is slower from the shock wave theory, by an approximate factor of $\frac{2}{\gamma+1}$ [40]. Thus the axial elongation of the CS is;

$$\frac{dz_s}{dt} = -\frac{2}{\gamma + 1} \frac{dr_s}{dt} \tag{4.26}$$

Radial piston motion

We assume an adiabatic relationship to a fixed mass of gas in the slug during the incremental motion dr_s.

We have,

$$PV^\gamma = constant \tag{4.27}$$

or

$$\frac{\gamma dV}{V} + \frac{dP}{P} = 0 \tag{4.28}$$

where slug pressure

$$P \sim V_s^2 \text{ So}, \frac{dP}{P} = 2(\frac{dI}{I} - \frac{dr_p}{r_p}) \tag{4.29}$$

This amount swept in is equal to the ambient gas swept through by the shock front in it's motion dr_s. This swept-up gas is compressed by a ratio $\frac{\gamma+1}{\gamma-1}$ and will occupy part of increase in volume dV [20].

The actual increase in volume available to the original mass of gas in volume V does not correspond to increment dr_s but to an effective increment $dr_s(\frac{2}{\gamma+1})$. (Note γ is specific heat ratio of the plasma. Eg. $\gamma = \frac{5}{3}$ for atomic gas,$\gamma = \frac{7}{5}$ for molecular gas; for strongly ionizing argon γ has value closer to 1 (as1.15)) [41].
Thus, the more correct interpretation is;

$$dV = 2\pi(r_P dr_p - \frac{2}{\gamma+1} r_s dr_s) z_f + \pi(r_p^2 - r_s^2) dz_f \tag{4.30}$$

Thus we have;

$$\frac{\gamma dV}{V} = [2\gamma(r_p dr_p - \frac{2}{\gamma+1} r_s dr_s) z_f + \gamma(r_p^2 - r_s^2) dz_f]/[z_f(r_p^2 - r_s^2)] \tag{4.31}$$

Now, adding together $\frac{dP}{P}$ and $\frac{\gamma dV}{V}$. We will have after rearranging and putting dr_p as the subject we have,

$$\frac{dr_p}{dt} = [\frac{2}{\gamma+1}\frac{r_s}{r_p}\frac{dr_s}{dt} - \frac{r_p}{\gamma I}(1 - \frac{r_s^2}{r_p^2})\frac{dI}{dt} - \frac{1}{\gamma+1}\frac{r_p}{z_f}(1 - \frac{r_s^2}{r_p^2})\frac{dz_f}{dt}]/[\frac{\gamma-1}{\gamma} + \frac{1}{\gamma}\frac{r_s^2}{r_p^2}] \tag{4.32}$$

where, we are reminded that, r_p is the radial piston position, r_s is the radial shock front position and z_f is the axial piston position.

Circuit equation during radial phase

The inductance of the focus tube now consists of the full inductance of the axial phase and

the inductance of the radially imploding and elongating plasma pinch [37].

Thus,

$$L = \frac{\mu_0}{2\pi}(\ln c)z_0 + \frac{\mu_0}{2\pi}(\ln \frac{b}{r_p})z_f \tag{4.33}$$

Here both z_f and r_p vary with time. Thus on substituting. We will have from the circuit equation above as;

$$\frac{dI}{dt} = [V_0 - \frac{\int I dt}{C_0} - Ir_0 - f_c\frac{\mu_0}{2\pi}(\ln \frac{b}{r_p})I\frac{dz_f}{dt} + f_c\frac{\mu_0}{2\pi}\frac{z_f}{r_p}I\frac{dr_p}{dt}]/[L_0 + f_0\frac{\mu_0}{2\pi}(\ln c)z_0 + f_c\frac{\mu_0}{2\pi}(\ln \frac{b}{r_p})z_f] \tag{4.34}$$

These above four equations from (4.25) to (4.34) are the generating equation form a close set of equations. These can be integrated for the value of r_s, r_p, z_f and I. For the simplicity the above generating equation are normalized with adopting the following condition;

$\tau = \frac{t}{t_0}$, $\iota = \frac{I}{I_0}$ as in the axial phase but with $\kappa_s = \frac{r_s}{a}$,$\kappa_p = \frac{r_p}{a}$ and $\zeta_f = \frac{z_f}{a}$ the distances are normalized to anode radius, instead of anode length [39]. After normalization the above generating equations becomes as,

Radial shock speed:

$$\frac{d\kappa_s}{d\tau} = -\alpha\alpha_1\frac{\iota}{\kappa_p} \tag{4.35}$$

Axial column elongation speed (both ends of the column defined by axial piston):

$$\frac{d\zeta_f}{d\tau} = -\frac{2}{\gamma+1}\frac{d\kappa_s}{d\tau} \tag{4.36}$$

Radial piston speed:

$$\frac{d\kappa_p}{d\tau} = [\frac{2}{\gamma+1}\frac{\kappa_s}{\kappa_p}\frac{d\kappa_s}{d\tau} - \frac{\kappa_p}{\gamma\iota}(1-\frac{\kappa_s^2}{\kappa_P^2})\frac{d\iota}{d\tau} - \frac{1}{\gamma+1}\frac{\kappa_p}{\zeta_f}(1-\frac{\kappa_s^2}{\kappa_p^2})\frac{d\zeta_f}{d\tau}]/[\frac{\gamma-1}{\gamma} + \frac{1}{\gamma}\frac{\kappa_s^2}{\kappa_p^2}] \tag{4.37}$$

Current :

$$\frac{d\iota}{d\tau} = [1 - \int \iota d\tau + \beta_1[\ln(\frac{\kappa_p}{c})]\iota\frac{d\zeta_f}{d\tau} + \beta_1\frac{\iota\zeta_f}{\kappa_p}\frac{d\kappa_p}{d\tau} - \delta\iota]/[(1+\beta-\beta_1[\ln(\frac{\kappa_p}{c})]\zeta_f)] \tag{4.38}$$

where, the scaling parameters are introduced as,

$$\beta_1 = \frac{\beta}{F\ln(c)} \tag{4.39}$$

With

$$F = \frac{z_0}{a} \tag{4.40}$$

and

$$\alpha_1 = \sqrt{\frac{(\alpha+1)(c^2-1)}{(4\ln(c))}} F \sqrt{\frac{f_m}{f_{mr}}} \tag{4.41}$$

Above, we interpret $\alpha = \frac{t_0}{t_a}$ and $\alpha_1 = \frac{t_a}{t_r}$; which gives $\alpha\alpha_1 = \frac{t_a}{t_r}$ where, α_1 is the ratio of characteristic axial transit to characteristic radial compression inward shock transit time.

The characteristic speed of inward shock to reach focus axis is ;

$$\upsilon_r = \frac{a}{t_r} = \frac{\sqrt{\mu_0(\gamma+1)}}{4\pi} \frac{f_c}{\sqrt{f_{mr}}} \frac{\frac{I_0}{a}}{\sqrt{\rho}} \tag{4.42}$$

The ratio of characteristic radial and the axial speeds is also essentially a geometrical one, modified by thermodynamics with a typical value 2.5 [39].

calculation of voltage V across PF input terminals

As we have

$$V = \frac{d(LI)}{dt} \tag{4.43}$$

Putting the value of L and expressing in the normalizing form.

$$\upsilon = [\beta - \beta_1(\ln\frac{\kappa_p}{c})\zeta_f]\frac{d\iota}{d\tau} - \beta_1\iota[(\frac{\zeta_f}{\kappa_p})\frac{d\kappa_p}{d\tau} + (\ln\frac{\kappa_p}{c})\frac{d\zeta_f}{d\tau}] \tag{4.44}$$

Integrating the above equations with the initial conditions; τ = time that axial phase ended, $\kappa_s = 1$,$\kappa_p = 1$ and $\zeta_f = 0$, ι = value of current at the end of the axial phase and $\int \iota d\tau$ = value of "flowed charge" at the end of the axial phase with taking smaller time increment of $D = \frac{0.001}{100}$.

Next step values are computed by using the method of linear approximations. That enables us to compute the new generating values and the sequence is repeated step by step until $\kappa_s = 0$.

In the slug model it was assumed that the pressure exerted by the magnetic piston is instantaneously felt by the shock front (position r_s). Likewise the shock speed dt dr_s is instantaneously felt by the piston (CS). This assumption of infinite small disturbance speed (SDS) is implicit in equations (4.25) and (4.32) (or in normalized form (4.35) and (4.37)). Since the SDS is finite, there is actually a time lapse At communicating between the SF and CS.

Which lead to the correction in the numerical values that's why effected values are changed (as example; ι is changed to (ι_{delay}), κ_p is changed to $(\kappa_p)_{delay}$ in equation (4.35) and in equation (4.37) $\frac{d\kappa_s}{d\tau}$ is replaced by $(\frac{d\kappa_s}{d\tau})_{delay}$) [39].

4.3.2 Radial reflected shock phase

When the inward radial shock hits the axis $\kappa_s = 0$. Thus in the computation, when $\kappa_s \leq 1$ the radial inward phase goes towards radial reflected shock phase.

Then we start to compute radial reflected shock(RS) phase and is given a constant speed of 0.3 times the on-axis inward shock speed.

So, Reflected Shock Speed

$$(\frac{dr_s}{dt}) = -0.3(\frac{dr_s}{dt}) \tag{4.45}$$

Negative sign shows that the direction of the on- axis inward shock (position r_p) and the RS(position r_r) is opposite. Which moves outwards and on-axis inward shock moves inward. Eventually r_r increases until it value reaches the decreasing value r_p.

The piston speed is same as in the radial inward shock phase with $r_s = 0$ and $\frac{dr_s}{dt} = 0$. The Elongation speed and tube voltage are same as in the radial inward shock phase [40].

4.3.3 Slow compression phase

This Phase is responsible for the emission of the radiation. In this phase the piston speed is:

$$\frac{dr_p}{dt} = [-\frac{r_p}{I\gamma}\frac{dI}{dt} - \frac{1}{\gamma+1}\frac{r_p}{z_f}\frac{dz_f}{dt} + \frac{4\pi(\gamma-1)}{\mu_0\gamma z_f}\frac{r_p}{f_c^2 I^2}\frac{dQ}{dt}]/[\frac{\gamma-1}{\gamma}] \tag{4.46}$$

Here, we have included energy loss/gain terms into the equation of motion. The plasma gains energy from Joule heating; and loses energy through Bremstralung, Recombination and line radiation. Energy gain term will end to push the piston outwards and loss term will have the opposing effect [37].

The Joule energy gain can be presented as;

$$\frac{dQ_J}{dt} = RI^2 f_c^2 \tag{4.47}$$

where,

$$R = \frac{1290 Z z_f}{\pi r_p^2 T^{\frac{3}{2}}} \tag{4.48}$$

with

$$T = \frac{\mu_0}{8\pi^2\kappa}\frac{I^2 f_c^2}{D N_0 a^2 f_{mr}} \tag{4.49}$$

The Bremsstralung loss term, Recombination loss term and the Line loss term are given below respectively as;

$$\frac{dQ_B}{dt} = -1.6 \times 10^{-40} N_i^2 (\pi r_p^2) z_f T^{\frac{1}{2}} Z^3 \tag{4.50}$$

$$\frac{dQ_{rec}}{dt} = -5.92 \times 10^{-35} N_i^2 (\pi r_p^2) Z \frac{z_f}{T^{\frac{1}{2}}} \tag{4.51}$$

and

$$\frac{dQ_L}{dt} = -4.6 \times 10^{-31} N_i^2 (\pi r_p^2) Z Z_n^4 \frac{z_f}{T}, \tag{4.52}$$

where $N_0 = 6 \times 10^{26} \frac{\rho_0}{M}$ and $N_i = N_0 f_{mr} (\frac{a}{r_p})^2$

Then we will get the net gain/ loss of the plasma column is as;

$$\frac{dQ}{dt} = \frac{dQ_J}{dt} + \frac{dQ_B}{dt} + \frac{dQ_{rec}}{dt} + \frac{dQ_L}{dt} \tag{4.53}$$

For the calculation of the soft x-ray (SXR) yield it was taken that $Y_{XSR} = Q_L$ and in the above equation Z_n is the atomic number of the gas used there and the value of Q_L is obtain by integrating over the pinch duration and SXR energy generated within the plasma pinch depends on the number density N_i, effective charge number Z, pinch radius r_p, pinch length z_f and the temperature T [37].

Column Elongation speed

Here it was adopted that the elongation to be driven fully by the plasma pressure.

So,

$$\frac{dz_f}{dt} = \sqrt{\frac{\mu_0 \gamma + 1}{\rho_0}} \frac{I f_c}{4\pi r_p} \tag{4.54}$$

And also the Circuit current equation is;

$$\frac{dI}{dt} = [V_0 - \frac{\int I dt}{C_0} - I(R f_c + r_0) - f_c \frac{\mu_0}{2\pi} (\ln \frac{b}{r_p}) I \frac{dz_f}{dt} + f_c \frac{\mu_0}{2\pi} \frac{z_f}{r_p} I \frac{dr_p}{dt}] / [L_0 + f_c \frac{\mu_0}{2\pi} (\ln c) z_0 + (\ln \frac{b}{r_p}) z_f] \tag{4.55}$$

The voltage across focus terminals is;

$$V = \frac{\mu_0 f_c}{2\pi} I [(\ln \frac{b}{r_p}) \frac{dz_f}{dt} - \frac{z_f}{r_p} \frac{dr_p}{dt}] + \frac{\mu_0 f_c}{2\pi} [(\ln \frac{b}{r_p}) z_f + (\ln C) z_0] \frac{dI}{dt} + RI \tag{4.56}$$

The above generating equations are integrated to find out the value of the z_f, r_p and I with the help of neutralization and in each of the step the net power gain/loss can be calculated. The final result of this instability mechanism is the breaking up of the focus pinch into a large expanded current column [37].

4.3.4 Expanded column axial phase

In the expanded column phase it was assumed that the current flows uniformly from anode to cathode in a uniform column having the same radius as the anode and a length of z.

The normalized equations for this phase are given as follow (which are obtain by same process as in the axial phase);

Circuit (Current) Equation :

$$\frac{d\iota}{d\tau} = \frac{1 - \int \iota d\tau - \beta\iota\frac{d\zeta}{d\tau}e - \delta\iota}{1 + \beta + \beta(\zeta - 1)e} \tag{4.57}$$

where,

$$e = \frac{[\ln c + \frac{1}{z}]}{\ln c} \tag{4.58}$$

Equation of motion :

$$\frac{d^2\zeta}{d\tau^2} = \frac{\alpha^2\iota^2 e_1 - h^2(\frac{d\zeta}{d\tau})^2}{1 + h^2(\zeta - 1)} \tag{4.59}$$

where,

$$e = \frac{[\ln c + \frac{1}{4}]}{\ln c} \tag{4.60}$$

and

$$h = \sqrt{\frac{c^2}{(c^2 - 1)}} \tag{4.61}$$

The initial conditions for ι and $\int \iota d\tau$ are the last values of ι and $\int \iota d\tau$ from the slow compression phase. The initial value of ζ is $\zeta = 1 + \zeta_f$, where ζ_f is the last length of the focus column, but normalized to z_0 rather than z [39].

It is noted that the transition from Phase 4 to 5 is observed in laboratory measurements to occur in an extremely short time with plasma/current disruptions, resulting in localized regions of high densities and temperatures.

4.4 NX2 Plasma Focus Device

NX2 is a second system designed and constructed at Singapore with anode diameter 4 cm and cathode diameter 8 cm made of stainless steel. The length of the anode is kept 5 cm

and 7 cm and is 3kJ four module system with a peak current 420 kA at 11.5 kV. Water is circulated through the electrodes using two Bay voltex RRS-1650-AC chillers with a cooling capacity and operated at peak into water-cooled electrodes at repetitive rated up to 20 Hz to produce 300 W SXR in burst durations of up to 5 minutes.

SXR lithographs are taken from NX2 and to demonstrate the SXR lithographs sufficient SXR flux is generated for an exposure with only 300 shots. Furthermore, flash electron lithographs are also obtained which require only 10 shots per exposure. Such high performance compact machines may be improved to yield over 2 kW of SXR, enabling sufficient exposure throughput to be of interest to the water industry. Figure 4.2 shows schematic of the electrical system and Schematic of focus electrodes and chamber of NX2 device [42, 43].

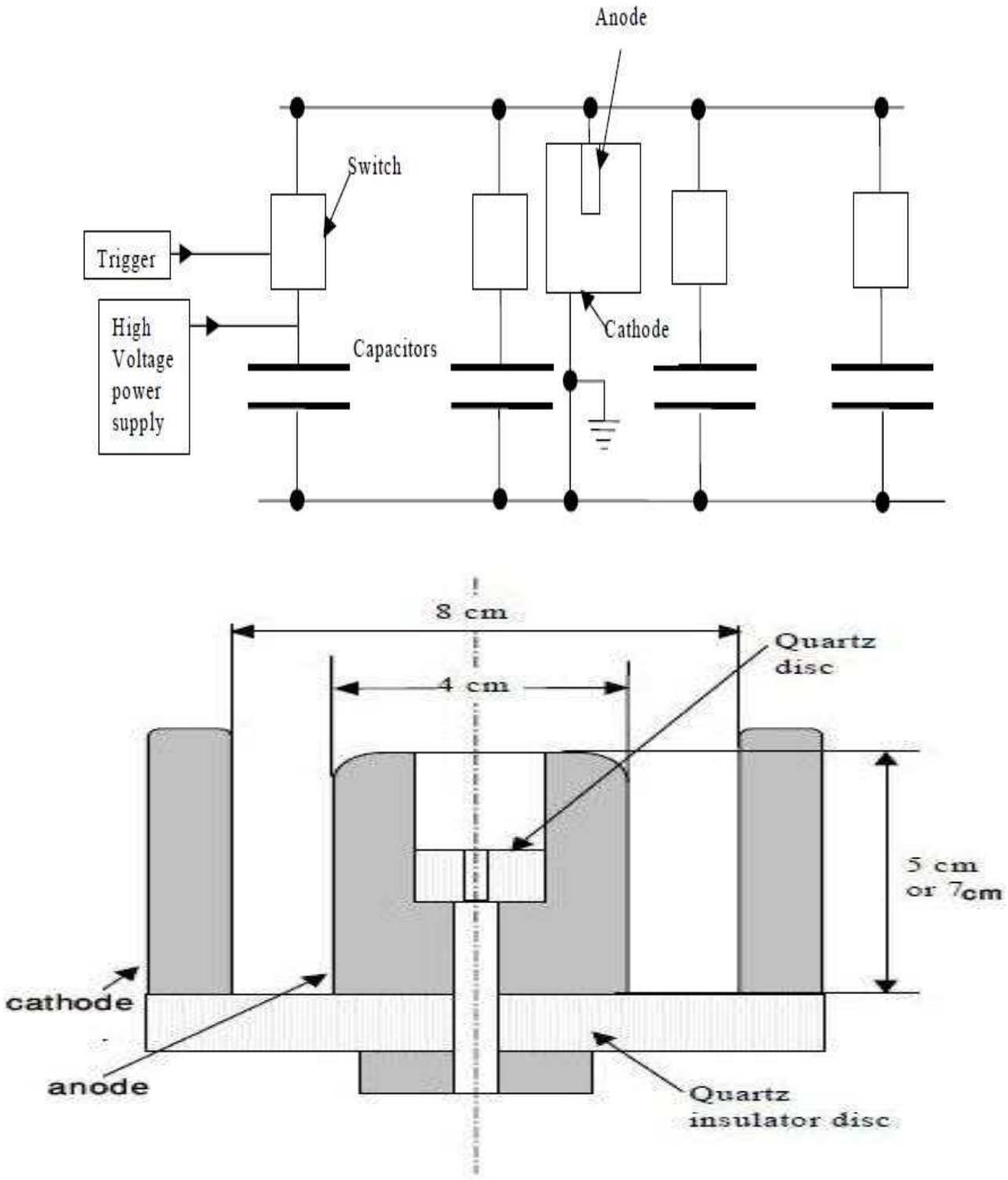

Figure 4.3: *Schematic of the electrical system and Schematic of focus electrodes and chamber [42, 43].*

Chapter 5

Results and Discussion

As discussed in chapter 4, neon soft x-ray yield (Y_{sxr}) on NX_2 machine is to be equivalent to line radiation loss term (Y_{sxr} =Q_L) and can be obtained by integrating equation (4.52) over the pinch duration. The generated energy is then reduced by the plasma Self-absorption, which vitally depends on temperature and on the density; the reduced quantity of energy is then emitted as the soft x-ray (SXR) yield. The SXR was first observed by Liu [18] that at the temperature around 300 eV. According to Liu this temperature range is maximum for the production of SXR from neon operated plasma. Bing's subsequent work suggest that it around 2×10^6K (below 200 eV) [16] and the result obtained by using Lee Model code approaches very close to the result of the Bing. Hence for Neon SXR scaling there is an optimum small range of temperatures (T window) to operate [22].

To start numerical experiments a discharge current trace of the NX_2 is taken with a Rogowski coil as the reference trace [42, 43]. The selected measured waveform is of a shot at 2.6 Torr neon, near optimum Y_{sxr} yield, where bank parameters are taken as; static inductance $(L_0) = 15nH$, capacitance $(C_0) = 2.8\mu F$, stray resistance $(r_0) = 2.2m\Omega$, tube parameter as; cathode radius $(b) = 4.1cm$, anode radius $(a) = 1.9cm$, anode length $(z_0) = 5cm$ and operation parameters as; voltage $(V_0) = 11KV$, pressure $P_0 = 2.6$ Torr. The nature obtained from the numerical experiment method is compared with the experimentally measured plot taken from the figure of 7(b) of the article published in Lee et al of [42, 43]. These are plotted to compare the data obtained by numerical experimental data obtained using Lee Model Code.

The computed total current waveform is fitted with the measured one with varying the parameters one by one. Fine tuning of the wave form is found to be at the values; $f_m = 0.1$, $f_c = 0.7$, $f_{cr} = 0.68$ and $f_{mr} = 0.12$. These values are used for the computation of all other discharges at various pressure. The Lee Model Code is used for each pressure starting at high pressure (1000000 Torr) and the discharge at this pressure is taken as the short circuit discharge because it stayed at the back wall without any motion. Then the pressure is lowered for the next run. This process is continued each time with new lowered pressure

of the neon. Table 5.1 and Table 5.2 shows the different plasma dynamics for some of the pressure starting from 5 to 0.2 Torr on this range the Y_{sxr} ranges from maximum to zero or minimum. The figure 5.1 shows the discharge current wave forms for some of the selected pressures from that it can be noticed the computed total current waveform at neon pressure 2.6 Torr is almost identical to the measured waveform for total current at neon pressure 2.6 Torr actual experiment conducted by Zhang [42, 43].

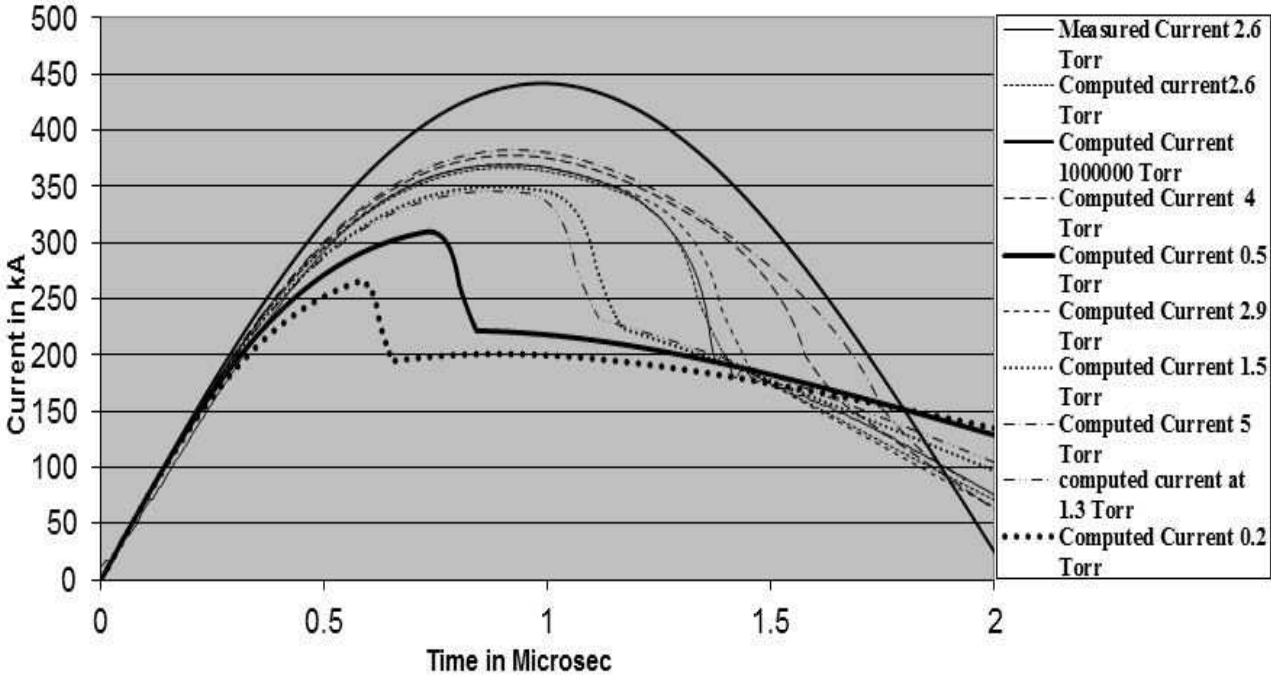

Figure 5.1: *Total current waveform of numerical experiment conducted at 2.6 Torr of neon and that of experimentally measured waveform at same 2.6 Torr of neon is plotted for comparison shows the fine tuning. Plots of discharge current waveforms from numerical experiments performed over gas filling pressure from 0.2 Torr to 5 Torr Measured data are from the article of Lee et al [42, 43] published in 7[b].*

Total current waveform shows the uploaded high pressure discharge waveform reaches at peak is about 442 kA just before $1\mu s$. At 5 Torr, the peak of the total current I_{peak} is 383 kA and a small current dip is seen at 1.78 μs which is well after peak current with the total discharge current having dropped to 152 kA at the start of the dip. Other corresponding values of I_{peak} decreases progressively with successive decrease of the neon pressure. On the

other hand the current dip appears more earlier times than the preceding one. At pressure 1.3 Torr I_{peak} dropped to 346 kA and the dip start almost at about the time peak current of the high pressure shot. Table 5.1 and Table 5.2 show pinch plasma dynamics function of the pressure as computed by numerical experiments. From table it is clearly seen that at 2.9 Torr Y_{sxr} is maximum and all the values above obtained are normalized to its value at optimum to plot all the properties in one graph. The normalized pinch parameters and absolute Y_{sxr} are then plotted as a function of filling gas pressure. The real experimental plot also included for comparison and that values are taken from [42, 43].

The real experiment was performed with the pressure of 2.9 Torr with 11.5 kV and having anode length 5 cm. Table 5.1 and Table 5.2 shows the real experimental value reasonably fit well.

Figure 5.2 presents the graph of different pinch plasma dynamics (I_{peak} *is the peak value of the total discharge current;* I_{pinch} *is the pinch current which is taken at the start of the pinch phase;* a_{min} *is the minimum pinch radius or known to be the radius at maximum compression; pinch duration and in the table listed as pnch dur; plasma temperature at middle of the pinch duration(*T_{pinch}*);* n_i *pinch as the ion density at the middle of the pinch duration and* Z *is the charge of the neon at the middle of the pinch duration*) versus filling neon pressure ranging from 5 Torr to 0.2 Torr. All parameters are normalized by respective values of the parameter obtained for the gas pressure 2.9 Torr. The line graphs are intersected at 2.9 Torr because of normalization.

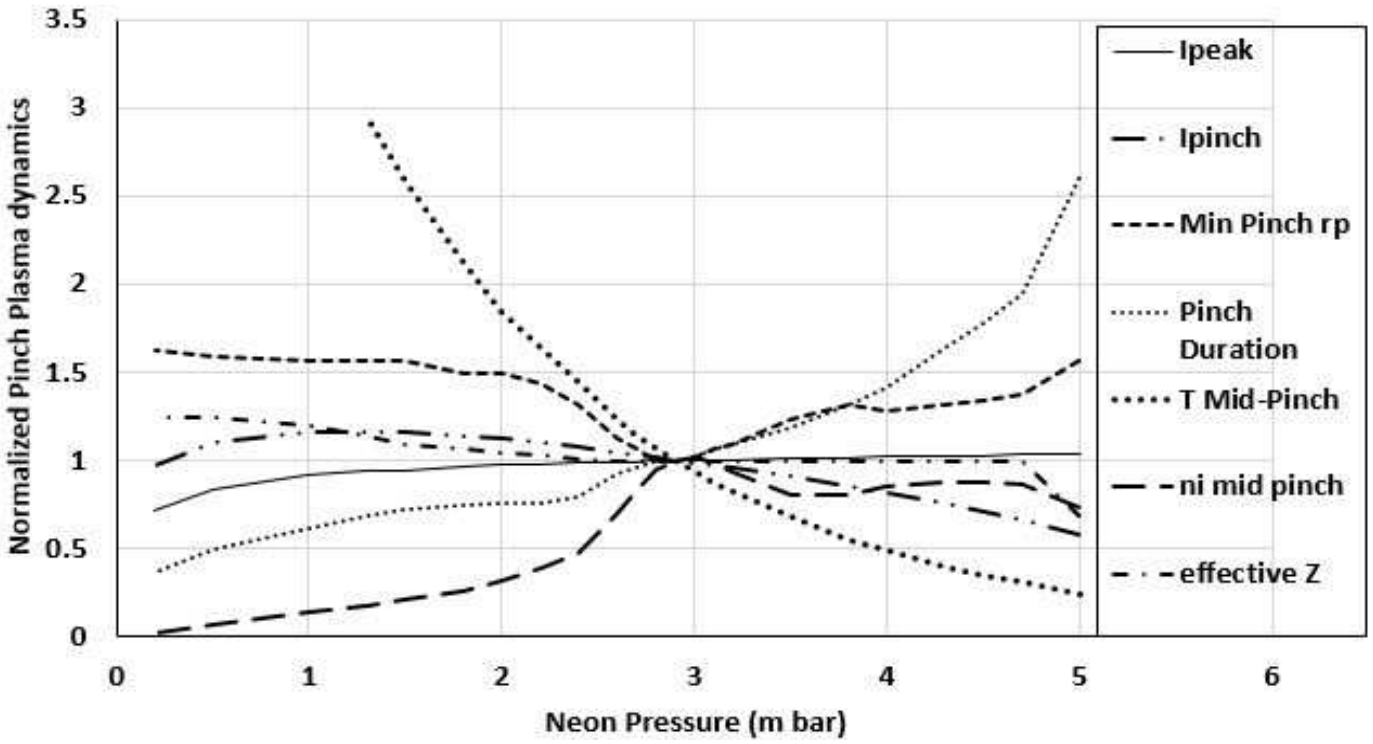

Figure 5.2: *Effect on some key pinch plasma parameters of operating gas pressure (all normalized using value at optimum operating pressure of 2.9 Torr neon pressure).*

Figure 5.3 presents Y_{sxr} versus neon pressure the effect of operating gas pressure on Y_{sxr}. The solid line shows for the values estimated by using the numerical experiment using Lee model Code. From Table 5.2 it is clearly seen that the maximum value of Y_{sxr} is 22.6 at neon pressure 2.9 Torr and the minimum is zero at 0.2 Torr. The Y_{sxr} decreases on increasing and decreasing neon pressure. The dotted plot is for the experimentally measured values for Y_{sxr} of NX_2 operated under similar conditions at the laboratory and is included for comparison.

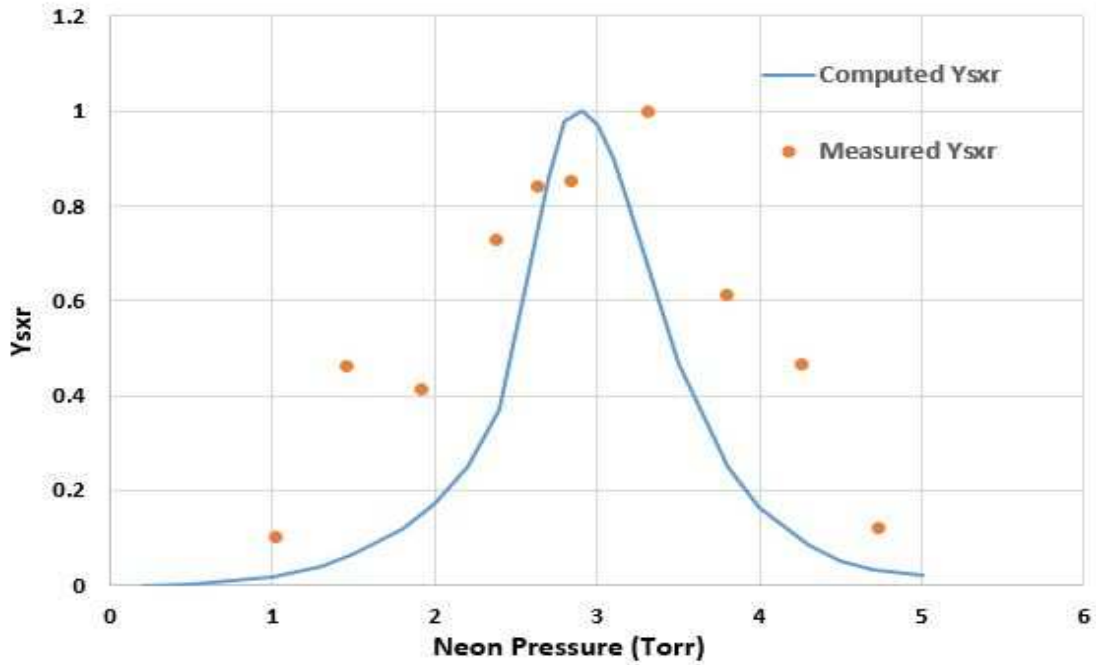

Figure 5.3: Y_{sxr} *versus neon pressure*

Computed plasma dynamics and pinch plasma parameters for different neon filling gas pressures by numerical experiments conducted on NX2 device using Lee model code are plotted in *TABLE 5.1 and TABLE 5.2.*

Parameters and the dynamics used in the following **TABLE 5.1** *are:* I_{peak} *is the peak value of the total discharge current;* I_{pinch} *is the pinch current and value is at start of the pinch; peak* v_a*=peak axial speed; S=speed parameter in* $(kA/cm/Torr^{1/2})$*; peak* v_s*,* v_p*=peak radial shock and piston speeds, respectively;* a_{min}*=minimum radius or focus pinch radius at maximum compression;* z_{max}*=maximum length of focus pinch at time of maximum compression and in* **TABLE 5.2** *are; pnch dur = pinch duration;* V_{max} *= maximum potential at the middle of the pinch duration;* T_{pinch}*= plasma temperature at middle of pinch duration;* n_i *pinch=ion density at the middle of pinch duration; Z=effective charge of the neon plasma at middle of pinch duration; EINP=work done by the dynamic resistance during radial phase expressed as; EINP %;* Y_{sxr} *=the soft x-ray yield and ALT= ratio of characteristic capacitor time to sum of characteristic axial and radial times. All the parameters of Table 5.1 and Table 5.2 are numerically calculated using the Lee Model Code for the successive decrease of the pressure*

starting from 5 Torr to 0.2 Torr. Table 5.3 presents the normalized real experimental data

TABLE 5.1

P_0	I_{peak}	I_{pinch}	Peak v_a	S	Peak v_s	Peak v_p	a_{min}	z_{max}
Torr	kA	kA	$\frac{cm}{\mu s}$		$\frac{cm}{\mu s}$	$\frac{cm}{\mu s}$		
5	383	84	4.3	90	11	8.6	0.25	2.7
4.7	381	96	4.5	93	12	9.4	0.22	2.6
4.5	380	103	4.6	94	12.8	10	0.21	2.7
4.3	379	109	4.7	96	13.5	10.6	0.21	2.7
4	378	118	4.9	99	14.9	11.6	0.21	2.7
3.8	376	124	5	102	15.9	12.1	0.21	2.7
3.5	374	132	5.3	105	17.3	12.9	0.20	2.7
3.2	372	139	5.5	109	18.8	13.7	0.17	2.8
3.1	371	141	5.6	111	19.3	14	0.17	2.8
3	370	143	5.7	113	19.9	14.2	0.16	2.8
2.9	369.4	145	5.8	114	20.5	14.5	0.16	2.79
2.8	368	147	5.9	116	21.1	14.8	0.16	2.8
2.7	367	149	6	118	21.8	15	0.17	2.8
2.6	366	152	6.1	120	22.5	15.3	0.18	2.8
2.4	364	156	6.3	124	24.4	15.8	0.21	2.7
2.2	362	159	6.5	128	24.7	16.3	0.23	2.7
2	359	163	6.8	134	25.3	16.8	0.24	2.7
1.8	356	165	7.1	140	26	17.3	0.24	2.7
1.5	350	168	7.6	151	27.6	18.9	0.25	2.75
1.3	346	169	8	160	29.1	20.2	0.25	2.8
1	337	169	8.8	178	32	22.8	0.25	2.8
0.5	310	160	11.1	231	40.8	29	0.25	2.8
0.2	265	140	14.7	312	55.7	38.4	0.26	2.7

TABLE 5.2

P_0	pnch dur	V_{max}	T pinch	n_i pinch	Z	ENIP%	Y_{sxr}	ALT
Torr	ns	KV	10^6 K(average)	$10^{26}/m^3$			Joule/shot	
5	78.6	6.9	0.4	4.2	5.5	18.5	0.46	0.61
4.7	58.8	8.8	0.5	4.9	8	19.7	0.73	0.63
4.5	53.8	10.1	0.56	5	8	20.5	1.15	0.644
4.3	49.5	11.5	0.65	5	8	21.4	1.89	0.659
4	42.5	13.7	0.79	4.9	8	22.7	3.66	.68
3.8	39.6	15	0.90	4.6	8	23.6	5.66	.701
3.5	35.7	16.9	1.11	4.6	8	25	10.54	0.73
3.2	33.1	18.7	1.34	5.3	8	26.4	18	0.76
3.1	32.1	19.2	1.42	5.6	8	26.8	20.28	0.776
3	30.9	19.8	1.53	5.8	8	27.2	21.93	.789
2.9	30.2	20.3	1.63	5.7	8	27.5	22.6	0.8
2.8	29.9	20.8	1.74	5.4	8	27.8	22.06	0.817
2.7	29	21.1	1.86	4.7	8	27.8	19.4	0.832
2.6	27.9	21.5	2	4	8	27.8	15.8	0.85
2.4	23.8	22.2	2.34	2.7	8.1	27.5	8.4	0.882
2.2	23	22.9	2.68	2.2	8.2	27.5	5.61	0.921
2	23	2.37	3	1.8	8.3	27.5	3.89	0.966
1.8	22.6	24.7	3.45	1.5	8.5	27.5	2.69	1.018
1.5	21.7	26.7	4.2	1.2	8.7	27.3	1.5	1.12
1.3	20.6	28.4	4.8	1	9.1	26.9	0.94	1.2
1	18.7	31.2	6.1	0.8	9.55	25.8	0.42	1.366
0.5	15.1	37	10.27	0.4	10	21.8	0.05	1.930
0.2	11	42	19.1	0.1	10	15.7	0	3.055

of Y_{sxr} and picked out from the article of Lee et al [42, 43] at [Fig. 6(b)]. All the values are normalized by the greatest value obtained to plot the all values within a graph to make our comparison more convenient.

Table 5.3

SN	Normalized Pressure	Normalized Y_{sxr}
1	1.02	0.101
2	1.92	0.413
3	1.46	0.463
4	2.378	0.728
5	2.63	0.839
6	2.84	0.853
7	3.31	1
8	3.8	0.612
9	4.26	0.467
10	4.74	0.119

Plot for radial phenomenon presents that the pinch axial elongation increases with increase of the time. Radial piston (current sheath) goes on decrease with increase in time after middle of the pinch duration. The radial inward shock goes on decreasing with time and reaches to minimum point after which, the radial reflected shock phenomena starts and goes on increasing with time. Slow compression phase started from the meeting point of the radial piston phenomena and the radial reflected shock phenomena. The currents sheath (radial piston) continues to move in slow compression phase after it hit the radial piston and reaches to the minimum pinch radius r_{min} at the end point of the slow compression phase. The computed graph agrees with the laboratory measured one [32].

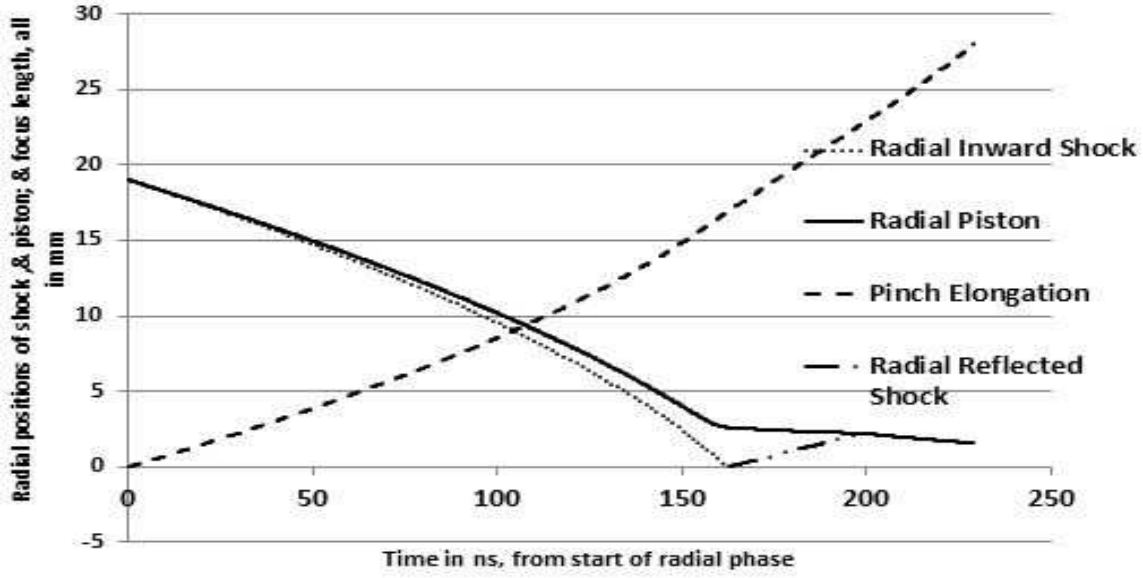

Figure 5.4: *Radial phases/phenomena (in mm) versus time (in ns)*

The plot for axial trajectories and speed versus time at the middle of the pinch duration we can clearly state that the axial trajectories and the speed at the middle of the pinch duration with time and goes on increasing with time. On increasing time there exist discontinuity, which separate the radial phenomena and the axial phenomena (before that discontinuity there will be the axial phenomena and after that there will be the radial one). At the missing section we are not calculating the axial phase portion of the current sheet during the radial phase which takes place at around $1.3 - 1.45\mu s$. The computed data and the graph exactly agrees the data obtained in the laboratory, this the computed one is compared with the published data at different paper at different time and by the different author [15, 22, 32].

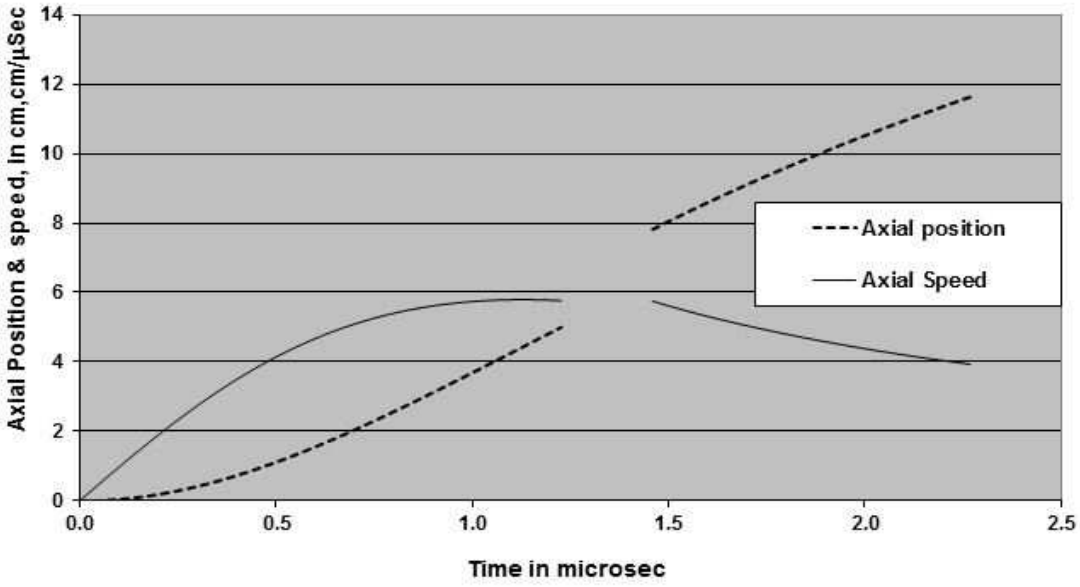

Figure 5.5: *Axial Trajectories and Speed versus time at the middle of the pinch duration*

The voltage plot shows that the voltage goes on increasing in the region of the radial phase with time, that is exponential up-to the maximum one and the value goes on sudden fall. The maximum value achieved at the mid pinch duration and was near about 150 ns. As the plasma self-absorption is included in the model but the contribution of the plasma self-absorption is not primary. The way of tube voltage fluctuation is reflective of the motor effect (induced voltages due to plasma current sheet motion in the various phases within the PF machine) [15, 32].

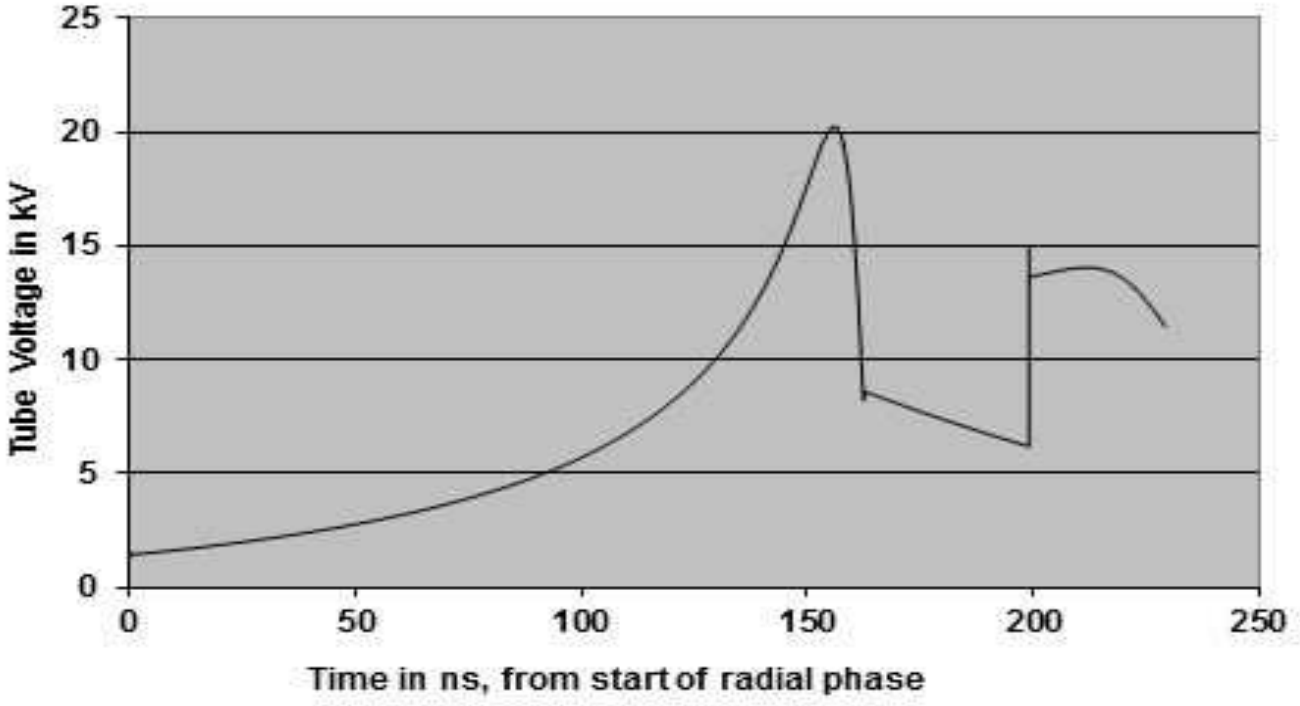

Figure 5.6: *The Tube voltage in kV from the start of the radial phase*

In the temperature graph the contribution of the plasma self-absorption is not primary. The plasma temperature versus time plot present the plasma temperature from the start of the radial phase and shows that goes on increasing with time till the middle of the pinch duration at which temperature is constant and then decreases with time at the last of the pinch duration. In the first section, temperature is calculated from shock speed. After it the directed motion is stopped due to reflected shock (RS) mechanism and causes the vertical jump (factor nearly equal to two). In the model RS temperature is taken as the constant from on-axis value as RS moves radially outwards until it hits the radially incoming piston, which results the flat top in the temperature graph [15, 32].

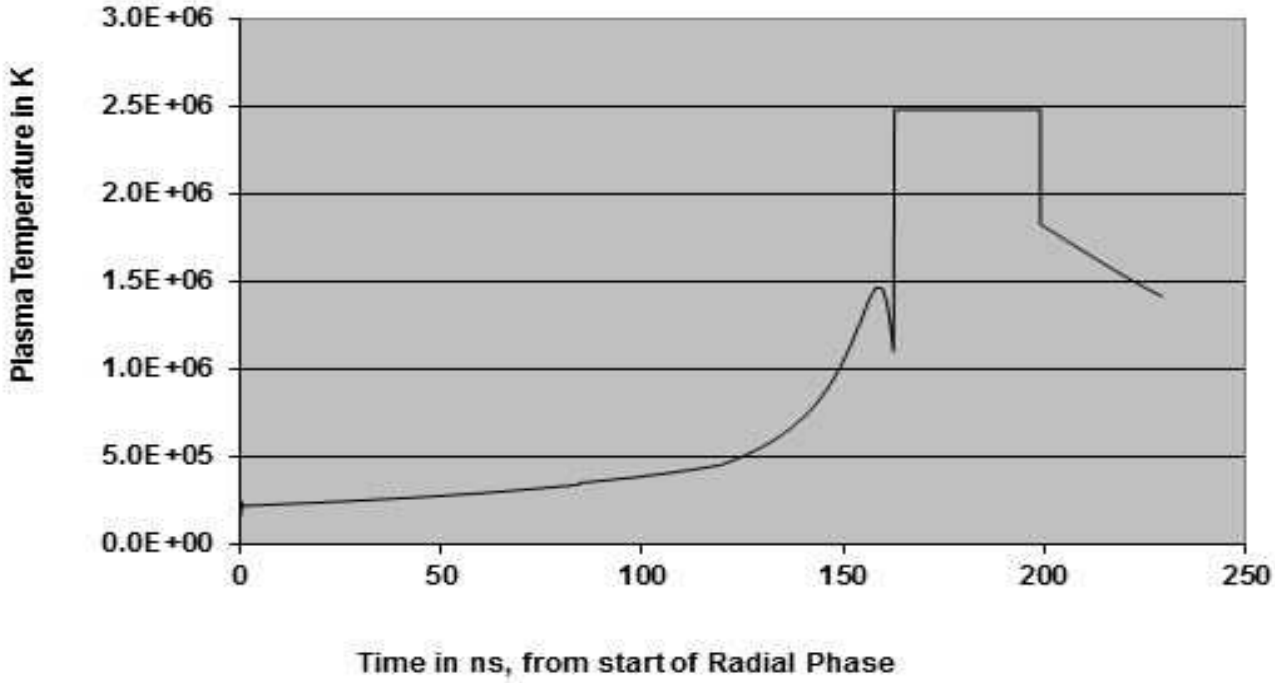

Figure 5.7: *Plasma Temperature from start of the radial phase in K versus time in ns*

Chapter 6

Conclusion and Future Works

6.1 Conclusion

The implementation of this Lee Model Code allowed us;

1. To study the radiation (x-ray) output
2. To determine the pinch lifetime
3. To compare the experimental data obtained by lab work and data predicted by Numerical method using Lee Model Code
4. To guide the radial implosion parameters(i.e axial and radial shock positions and speeds etc)

The topic of this dissertation is Soft x-ray yield from NX_2 plasma using PF. The studies on this aspects have been conducted numerically using Lee Model Code and the waveform is compared with the waveform obtained by plotting the experimentally obtained values (these values are picked from the waveform published in the different articles at different time).
The main task of this dissertation work is to study the soft $X-ray$ yield from NX_2 plasma as discussed above and our result shows the x-ray emission properties of NX_2 plasma. In the PF, plasma dynamics mainly determined by discharge current, anode and cathode electrodes geometry and the mass density of the gas which is filled-in control the final plasma temperature. The plasma dynamics also affected by ionization effect of the gas as here we use only one gas.
In conclusion this dissertation work shows that the Lee Model Code can be applied to perform numerical experiments to compute neon soft x-ray yield for NX_2 as a function of operating pressure. Figure 5.1 shows quite good agreement for the total current waveform by plotting at same graph with experimentally computed data and that agreed at pressure 2.9 torr with other variable same as for the experimental set up.
x-ray emission from PF carried out lots of operation with different pressure. Above table presented in chapter 5 clearly shows that there is the highest x-ray yield at the pressure of 2.6 Torr and the corresponding values parameter are used to normalize the values obtained at

different pressure value. Figure 5.3 shows the plot for the absolute soft x-ray yield (Y_{sxr}) and give the absolute maximum yield. Which also provide the reasonable degree of agreement between the estimated (Y_{sxr}) of NX_2 obtained by numerical experiments and the experimentally measured (Y_{sxr}) of NX_2 operated under the similar conditions.

Other several possible application fields can be readily identified to use electron beams like material processing, ablation, thin film deposition and surface modification etc.

6.2 Future Works

Finally, an experiment could be designed to solve the questions raised on our findings. The working can be further expanded with changing the working gas or after modifying the operating parameters (or using other set of operating parameters like voltage and pressure) or tube (design) parameters (anode radius, cathode radius, anode length) and bank parameters (static inductance, capacitance and stray resistance).

Other study can be performed to establish the role of the gas used in PF device in the emission of radiation (neutrons and x-rays). As this dissertation has shown, PF devices offer a wide research field for academic studies like in the study of plasma technology, x-ray emission through PF and to get wide knowledge about the plasma physics as well as on other diverse applications. Besides from these; PF device is relatively cheap device which offer excellent opportunities to train students in advanced physics diagnostics, x-ray, laser, electron technology etc.

Bibliography

[1] P. M. Bellan, *Fundamentals of Plasma Physics*, Cambridge University Press, Newyork, (2004)

[2] I. Langmuir, Phys. Rev., **33**, 954, (1929)

[3] W. Crookes, *Radiant Matter*, W. Queen and Company, Philadelphia, Newyork, (1878)

[4] F. F. Chen, *Introduction to Plasma Physics and Controlled Fusion*(Second edition), Plenum Press, New York, (1984)

[5] W. B. Thompson, *An Introduction to Plasma*, Pergamon Press, Newyork, (1962)

[6] J. A. Bittencourt, *Fundamentals of Plasma Physics*, Springer-verlag, London, (2004)

[7] U. Inan and M. Golkowski, *Principles of Plasma Physics for Engineers and Scientists*, Cambridge University Press, UK, (2011)

[8] F. F. Chen, Jane P. Chang, *Principles of Plasma Processing*, University of California, Los Angels, (2002)

[9] E. J. Lerner, Siam Physics Congress, (21-23 March, 2013)

[10] Burning Plasma Assessment Committee; Plasma Science Committee, *Burning Plasma: Bringing A Star to Earth*, The National Academies Press (www.nap.edu), Washington, DC (2004)

[11] M. Ariola and A. Pironti, *Magnetic Control of Tokamak Plasmas*, Springer-Verlag, London, (2008)

[12] J. D. Lawson, Proc. Phys. Soc., London, **B 70**, 6, (1957)

[13] S. Lee, T. Y. Tou, S. P. Moo, M. A. Eissa, A. V. Gholap, K. H. Kwek, S. Mulyodrono, A. J. Smith, S. Suryadi, W. Usada and M. Zakaullah, Amer. J. Phys., **56**, 1, (1988)

[14] S. Lee and S. H. Saw, *Nuclear Fusion Energy- The Dawning of the Fusion Age*, INTI International University (Malaysia) - Schools Outreach Programme in collaboration with

Institute for Plasma Focus Studies (Melbourne, Malaysia, Singapore)(archive accessed on 2013)

[15] S. Lee and S. H. Saw, *Nuclear Fusion Energy-Mankind's Gaint Step Forward; Invited Keynote paper: Second International Conference on Nuclear and Renewable Energy Resources*, Ankara, Turkey, (4-7 July 2010)

[16] B. Shan, *Plasma Dynamics and X-ray Emission of the Plasma Focus*; Ph.D. Dissertation, NIE, Nanyang Technological University, Singapore, (2000)

[17] R. Feder, J. S. Pearmann, J. C. Riordan and J. L. Costa, J. Microsc., **135**, 347 (1984)

[18] M. Liu, *Soft X-rays From Compact Plasma Focus*; Ph.D. dissertation,NIE, Nanyang Technological University, Singapore, (2006)

[19] A. Bernard, H. ruzzone, P. Choi, H. Chuaqui, V. Gribkov, K. Hirano, A. Krejci, S. Lee, C. M. Luo, F. Mezzetti, M. Sadowski, H. Schmidt, K. Ware, C. S. Wong and V. Zoita, *A Concept for an International Centre for Dense Magnetized Plasmas*; a proposal, prepared on the request of UNESCO, (1993)

[20] M. shahid, *Compression Dynamics and Radiation Emission From a Deuterium Plasma Focus*, Ph.D. dissertation, NIE, Nanyang Technological University, Singapore, (2000)

[21] S. Lee, J. Phys. D: Appl. Phys., **17**, 733, (1984)

[22] S. Lee, R. S. Rawat, P. Lee, and S. H. Saw, J. App. Physics, **106**, 023309 (2009)

[23] S. Lee, S. H. Saw, P. Lee and R. S. Rawat, Plasma Phys. Control. Fusion, **51**, 105013, (2009)

[24] S. Lee, S. H. Saw, R. S. Rawat, P. Lee, A. Talebitaher, A. E. Abdou, P. L. Chong, F. Roy, A. Singh, D. Wong, and K. Devi, IEEE Trans. Plasma Sci., **39**, 3196, (2011)

[25] M. S. Rafique, P. Lee, A. Patran, R. S. Rawat and S. Lee, J. Fusion Energy, **29**, 295, (2010)

[26] S. H. Saw, P. C. K. Lee, R. S. Rawat and S. Lee, IEEE Trans. Plasma Sci., **37**, 1276 , (2009)

[27] M. Akel, S. A. Hawat, S. H. Saw and S. Lee, J. Fusion Energy, **29**, 223, (2010)

[28] M. Akel, S. A. Hawat and S. Lee, J. Fusion Energy, **28**, 355, (2009)

[29] M. A. Mohammadi, S. Sobhanian, C. S. Wong, S. Lee, P. Lee and R. S. Rawat, J. Phys. D: Appl. Phys., **42**, 045203, (2009)

[30] A. C. Patran, *Electron and Medium Energy X-ray Emission From a Dense Plasma Focus*, Ph.D. dissertation, NIE, Nanyang Technological University, Singapore, (2002)

[31] S. S. Heoh, *Experimental Studies of a Current Stepped Z-Pinch*; Ph.D. Dissertation, University of Malaya, Kuala Lumpur, Malasiya,(1990)

[32] S. Lee, D. P. Subedi and S. H. Saw, *The Numerical Experiments Workshop on Plasma on Plasma Focus*, KU, Dhulikhel, Nepal, (26th September- 8th October 2013)

[33] S. Lee, S. P. Moo, C. S. Wong and A. C. Chew, *12 Years of UNU/ICTP PFF- A Review*, ICTP OAA report (1998), ICTP open access, (archive accessed on 2013)

[34] S. Lee, *Nuclear Fusion and the Plasma Focus; Invited Keynote paper: International Conference on Nuclear and Renewable Energy Resources*, Ankara, Turkey, (28-29 sept. 2009)

[35] S. Lee, S. H. Saw and J. Ali, J. Fusion Energy, **32**, 42, (2013)

[36] S. Lee, Ed. B. McNamara, **II**, 978, (1984)

[37] S. Lee, *Radiative Dense Plasma Focus Computation Package: RADPF (2008)*; IPFS open access, (archive accessed on 2013)

[38] S. Lee, *Scaling of the Plasma Focus - Viewpoint from Dynamics*, IPFS open access (archive accessed on 2013)

[39] S. Lee, *Radiative Dense Plasma Focus Computation Package: RADPF (2010)*; IPFS open access, (archive accessed on 2013)

[40] S. Lee, IEEE transactions on plasma science, **19**, 5, (1991)

[41] S. Lee, *Technology of a Small Plasma Focus Incorporating Some Experiences with the UNU/ICTP PFF*, Presented at the Symposium on Small Scale Laboratory Plasma Physics Experiments, Spring College on Plasma Physics, Italy, (15 May - 9 June 1989)

[42] S. Lee, P. Lee, G. X. Zhang, V. A. Gribkov, X. Feng, M. H. Liu and A. Serban, IEEE Trans. Plasma Sci., **26**, 4, (1998)

[43] S. Lee, P. Lee, G. X. Zhang, X. Feng, A. Serban, M. H. Liu, T. K. S Wong, C. Selvam and A. Thang,Proc. SPIE, **3183**, 277, (1997)